

Local Discontinuous Galerkin Methods with Decoupled Implicit-Explicit Time Marching for the Growth-Mediated Autochemotactic Pattern Formation Model

Hui Wang¹, Hui Guo², Jiansong Zhang³ and Lulu Tian^{4,*}

College of Science, China University of Petroleum, Qingdao, Shandong 266580, China

Received 14 August 2022; Accepted (in revised version) 14 February 2023

Abstract. In this paper, two fully-discrete local discontinuous Galerkin (LDG) methods are applied to the growth-mediated autochemotactic pattern formation model in self-propelling bacteria. The numerical methods are linear and decoupled, which greatly improve the computational efficiency. In order to resolve the time level mismatch of the discretization process, a special time marching method with high-order accuracy is constructed. Under the condition of slight time step constraints, the optimal error estimates of this method are given. Moreover, the theoretical results are verified by numerical experiments. Real simulations show the patterns of spots, rings, stripes as well as inverted spots because of the interplay of chemotactic drift and growth rate of the cells.

AMS subject classifications: 65M15, 65M60

Key words: Local discontinuous Galerkin methods, implicit-explicit time-marching scheme, error estimate, growth-mediated autochemotactic pattern formation model.

1 Introduction

Complex pattern appears in active systems, such as bacterial colonies, birds flocking, fish schools, insect swarms and other self-propelled particles [2, 9, 14, 15]. Several different mechanisms underlying pattern formation in bacteria have been explored, for example, temporal control of gene expression, density-dependent motility, quorum sensing, and the phenomenon of chemotaxis. The model we focus on in this paper was proposed by Mukherjee [13], which has shown interactions of bacterial growth kinetics, autochemotactic movement and cell movement. In addition, growth is a key adjustment parameter that can determine the spatiotemporal dynamics of a colony.

*Corresponding author.

Emails: CUOPWH@163.com (H. Wang), sdugh@163.com (H. Guo), jszhang@upc.edu.cn (J. Zhang), Tianll@upc.edu.cn (L. Tian)

Suppose $\Omega \subset \mathbb{R}^2$ be a rectangular domain. The growth-mediated autochemotactic pattern formation model [13] for self-propelling bacteria is demonstrated as follows in dimensionless form:

$$\frac{\partial \rho}{\partial t} = -\nabla \cdot (\rho \mathbf{p}) + \nabla^2 \rho + g\rho(1 - \rho), \tag{1.1a}$$

$$\frac{\partial c}{\partial t} = \mathcal{D}_c \nabla^2 c + \rho - c + \kappa \nabla \cdot (\rho \mathbf{p}), \tag{1.1b}$$

$$\frac{\partial \mathbf{p}}{\partial t} = -\Gamma \mathbf{p} + \mathcal{D}_p \nabla^2 \mathbf{p} + S \nabla c - \Gamma_2 |\mathbf{p}|^2 \mathbf{p}, \tag{1.1c}$$

where ρ is the bacterial density, c is the self-secreted chemical density, and $\mathbf{p} = (p_1, p_2)$ is the polarization. The variables and parameters in the model are defined as

$$|\mathbf{p}|^2 = p_1^2 + p_2^2, \quad g = \frac{\alpha}{k_d}, \quad \Gamma = \frac{\gamma}{k_d}, \quad \mathcal{D}_p = \frac{D_p}{D_\rho}, \quad \mathcal{D}_c = \frac{D_c}{D_\rho}, \quad \kappa = \frac{k_a k_d}{k_0 v_0} \quad \text{and} \quad \Gamma_2 = \frac{\gamma_2 D_\rho}{v_0^2},$$

where α is the growth rate, γ is the decay rate of \mathbf{p} , k_d denotes a rate of natural degradation, D_p and D_ρ are the translational diffusion constant and the diffusion constant, respectively, D_c is the diffusion constant, k_a is the anisotropic correction term, k_0 is the local rate, v_0 is the self-propulsion speed of the bacteria, γ_2 describes saturation in \mathbf{p} at strong alignment, g is the growth rate, and S is chemotactic strength. Here, the parameter S represents chemoattraction and chemorepulsion, for positive ($S > 0$) and negative ($S < 0$) values, respectively.

There are few of numerical simulations for the growth-mediated autochemotactic pattern formation model in self-propelling bacteria. In [13], the authors used the finite difference method to carry out numerical simulation, but there was no theoretical support for numerical analysis. When there is not any growth dynamics (i.e., $g = 0$), [10] explored a mass-preserving characteristic finite element approach, and the convergence analysis was well studied, yet only the first-order time scheme was developed. However, the circumstance that $g = 0$ is not particularly practical since bacteria density cannot expand locally in the absence of any bounds. Because the change in density is not minor, which is a characteristic of this problem in some circumstances, we must explore approaches with high resolution. As a result, for the model in this paper, we use local discontinuous Galerkin (LDG) methods. To the best of the authors' knowledge, this is the first paper that discusses error estimates for the model with this method.

Inspired by Bassi and Rebay [3], the LDG method was introduced by Cockburn and Shu [4] to solve the convection-diffusion equations. Thereafter, the LDG method has developed successfully and been employed in numerous models with higher-order and dispersive terms [21,22]. The principle of the LDG approach is to introduce certain auxiliary variables to reduce the higher-order derivatives in the equations to the first-order, so that the discontinuous Galerkin (DG) approach can then be used. Hence, the LDG approach inherits advantages of the DG method, including good stability, high-order precision, as well as flexibility on hp -adaptivity and complex geometry.

A main feature of this system is that a long time dynamical process is required before reaching the steady state. Therefore, the IMEX time-marching schemes will be adopted to resolve the problem in this paper. When solving linear convection-diffusion problems, the combination of IMEX time-marching with LDG spatial discretization was used in [18–20] to obtain good stability and accuracy. The IMEX scheme was further employed to incompressible miscible displacements in [21], and more recently, applied to the wormhole propagation [8], for good stability and accuracy.

There are three key issues in the theoretical analysis of our proposed methods. Firstly, the LDG method is employed for spatial discretization, so it is more difficult to carry out theoretical analysis because the inter-element discontinuities need to be resolved. According to Lemma 4.2, we leverage the link between the gradient and interface jump of the numerical solution with the approximation of auxiliary variable for the gradient in the LDG methods. Secondly, different from the traditional LDG method, we introduce new variables including both the convection and diffusion terms, otherwise it is tricky to obtain the error estimates. Thirdly, we will construct a new time marching method up to second-order accuracy to resolve the time level mismatch of the discretizations. It is essential to handle the nonlinear term $|\mathbf{p}|^2\mathbf{p}$ of the second-order time integration, so the values at time levels t^n, t^{n-1} are used to extrapolate the absolute value at time level $t^{n+\frac{1}{2}}$, which contributes to linearizing and decoupling the scheme, saving cost, and error estimates. Under weak temporal-spatial circumstances, we derive the optimal error estimates in $L^\infty(L^2)$ norm for density and polarization of both schemes. We simulate patterns of spots, stripes, rings and inverted spots, which indicates that our numerical method can account for both chemorepulsion and chemoattraction-related instabilities.

The rest of the paper is organized as follows. In Section 2, we provide a few preliminary setups, including assumptions, basic notations, definitions of norms and projections. In Section 3, we present two linear, decoupled time integrations. The error estimates for the time integrations are given in Section 4. The accuracy and capability of the method will be demonstrated by ample numerical simulations in Section 5. We end up with concluding remarks in Section 6.

2 Preliminaries

We demonstrate some preliminary settings to be used throughout the paper.

2.1 Hypotheses

The initial conditions of the system (1.1a)-(1.1c) are given as

$$\rho(x,y,0) = \rho_0(x,y), \quad \mathbf{p}(x,y,0) = \mathbf{p}_0(x,y), \quad c(x,y,0) = c_0(x,y), \quad (x,y) \in \Omega. \quad (2.1)$$

Throughout this paper, we focus on periodic boundary conditions for simplicity. However, there is not essential difficulty to extend the schemes to problems with homogeneous Neumann boundary.

Moreover, we give the following hypotheses (H) for the problem.

1. $0 < \rho_* \leq \rho(x, y, t) \leq \rho^*, 0 < c_* \leq c(x, y, t) \leq c^*$.
2. $g, \kappa, \Gamma, \Gamma_2, \mathcal{D}_c, \mathcal{D}_p$ are all given positive constants.
3. ρ, c and \mathbf{p} are uniformly bounded in $\mathbb{R}^2 \times [0, T]$.

2.2 Basic notations

Let $\Omega_h = \{K_{ij}\}$ be a partiton of $\Omega \subset \mathbb{R}^2$, where $K_{ij} = I_i \times I_j = (x_{i-1/2}, x_{i+1/2}) \times (y_{j-1/2}, y_{j+1/2})$, for $i = 1, 2, \dots, N_x, j = 1, 2, \dots, N_y$. For simplicity, if not otherwise stated, we always use K to denote a cell. We denote $h_i^x = x_{i+1/2} - x_{i-1/2}, h_j^y = y_{j+1/2} - y_{j-1/2}, \forall i, j$, and $h = \max_{i,j} \{h_i^x, h_j^y\}$. We assume the partitions are quasi-uniform in this paper, i.e., $h \leq \lambda \min_{i,j} \{h_i^x, h_j^y\}$, where λ is a positive constant independent of the mesh refinement.

The finite element spaces are defined as

$$\begin{aligned} \underline{\omega}_h &= \{ \underline{w} \in L^2(\Omega)^{2 \times 2} : \underline{w}|_K \in Q^k(K)^{2 \times 2}, \forall K \in \Omega_h \}, \\ \mathbf{M}_h &= \{ \mathbf{v} \in L^2(\Omega)^2 : \mathbf{v}|_K \in Q^k(K)^2, \forall K \in \Omega_h \}, \\ \chi_h &= \{ q \in L^2(\Omega) : q|_K \in Q^k(K), \forall K \in \Omega_h \}, \end{aligned}$$

where $Q^k(K)$ denotes the space of tensor product of polynomials of degrees at most k in K . They are subspaces of the broken Sobolev spaces $\underline{\omega} \times \mathbf{M} \times \chi$ shown below:

$$\begin{aligned} \underline{\omega} &= \{ \underline{w} \in L^2(\Omega)^{2 \times 2} : \underline{w}|_K \in H^1(K)^{2 \times 2}, \forall K \in \Omega_h \}, \\ \mathbf{M} &= \{ \mathbf{v} \in L^2(\Omega)^2 : \mathbf{v}|_K \in H^1(K)^2, \forall K \in \Omega_h \}, \\ \chi &= \{ q \in L^2(\Omega) : q|_K \in H^1(K), \forall K \in \Omega_h \}. \end{aligned}$$

We let $\mathbf{v} = (1, 1)^T$ be a fixed vector which is not parallel to any normals of the element interfaces. We denote by Γ_h the set of all element interfaces and $\Gamma_0 = \Gamma_h \setminus \partial\Omega$ the interior ones. Moreover, we define $e = \partial K_1 \cap \partial K_2 \subset \Gamma_0$ as an interior edge shared by the left element K_1 and the right element K_2 , with $\mathbf{v} \cdot \mathbf{n}_1 > 0$ and $\mathbf{v} \cdot \mathbf{n}_2 < 0$, where \mathbf{n}_1 and \mathbf{n}_2 are the outward normals of K_1 and K_2 , respectively. For any $q \in \chi_h$, we define $q^- = q|_{\partial K_1}$ and $q^+ = q|_{\partial K_2}$, respectively. The jump terms are defined as $[q] = q^+ - q^-$ for scalar functions, $[\mathbf{v}] = ([v_1], [v_2])^T$ for vector-valued functions, and $[\underline{w}] = ([w_{ij}])_{2 \times 2}$ for matrix-valued functions. Also, we denote $\partial\Omega_- = \{e \in \partial\Omega | \mathbf{v} \cdot \mathbf{n}_e < 0\}$, where \mathbf{n}_e is the outward normal of e , and $\partial\Omega_+ = \partial\Omega \setminus \partial\Omega_-$. For any $e \in \partial\Omega_-$, we denote $q^+|_e = q|_e$, and similarly, $q^-|_e = q|_e$ for $e \in \partial\Omega_+$. For convenience, given $e = \{x_{\frac{1}{2}}\} \times J_j \in \partial\Omega_-$ and $e' = \{x_{N_x + \frac{1}{2}}\} \times J_j \in \partial\Omega_+$, by the periodic boundary condition, we define

$$q^-|_e = q^-|_{e'} \quad \text{and} \quad q^+|_e = q^+|_{e'}.$$

Similarly, given $e = I_i \times \{y_{\frac{1}{2}}\} \in \partial\Omega_-$ and $e' = I_i \times \{y_{N_y+\frac{1}{2}}\} \in \partial\Omega_+$, we also define

$$q^-|_e = q^-|_{e'} \quad \text{and} \quad q^+|_e = q^+|_{e'}.$$

For more definition details, one can refer to [7].

We define several norms [17]: $\|q\|_\Lambda$ is the L^2 norm of q on the domain $\Lambda \subset \mathbb{R}^2$. $\|\cdot\|_{s,\Lambda}$ is the norm of the Sobolev space $H^s(\Lambda)$ for $s \geq 0$. If $\Lambda = \Omega$, the domain Ω will be omitted from subscripts for convenience. The similar norms of vector-valued function \mathbf{v} and matrix-valued function \underline{w} are given as

$$\|\mathbf{v}\|_{s,\Lambda} = \left(\sum_{i=1}^d \|v_i\|_{s,\Lambda}^2 \right)^{1/2} \quad \text{and} \quad \|\underline{w}\|_{s,\Lambda} = \left(\sum_{i,j=1}^d \|w_{ij}\|_{s,\Lambda}^2 \right)^{1/2}.$$

Some other norms are defined as follows

$$\|\mathbf{v}\|_{\Gamma_h} = \left(\sum_{e \in \Gamma_h} \|\mathbf{v}\|_e^2 \right)^{1/2}, \quad \|\underline{w}\|_{\Gamma_h} = \left(\sum_{e \in \Gamma_h} \|\underline{w}\|_e^2 \right)^{1/2} \quad \text{and} \quad \|\nabla \mathbf{v}\| = \left(\sum_{K \in \Omega_h} \|\nabla \mathbf{v}\|_K^2 \right)^{1/2}$$

for $\mathbf{v} \in \mathbf{M}_h$.

We denote Γ_K as the edges of K , and define

$$\|q\|_{\Gamma_K}^2 = \int_{\partial K} q^2 ds \quad \text{and} \quad \|q\|_{\Gamma_h}^2 = \sum_{K \in \Omega_h} \|q\|_{\Gamma_K}^2.$$

Additionally, let $\|q\|_{\infty,K}$ be the standard L^∞ norm of q in K , and

$$\|q\|_\infty = \max_{K \in \Omega_h} \|q\|_{\infty,K}.$$

Similar definitions apply to vector-valued and matrix-valued functions, and we omit the details to save space.

In this paper, the symbol C is employed as a generic constant independent of mesh size and time step, which may appear various values at various cases. Furthermore, the symbol ϵ denotes a small enough positive constant.

2.3 Projections

Firstly, we would like to introduce the classical inverse property [5].

Lemma 2.1. For $q \in \chi_h$, there exists $C > 0$ independent of h and q satisfying

$$h\|q\|_{\infty,K} + h^{1/2}\|q\|_{\Gamma_K} \leq C\|q\|_K.$$

Throughout this paper, several special projections will be used. We first would like to define a projection P^- onto χ_h [5]: for each cell K ,

$$\begin{aligned} (P^- \omega - \omega, \vartheta)_K &= 0, & \forall \vartheta \in Q^{k-1}(K), \\ \int_{J_j} (P^- \omega - \omega)(x_{i+\frac{1}{2}}, y) \vartheta(y) dy &= 0, & \forall \vartheta \in P^{k-1}(J_j), \\ \int_{I_i} (P^- \omega - \omega)(x, y_{j+\frac{1}{2}}) \vartheta(x) dx &= 0, & \forall \vartheta \in P^{k-1}(I_i), \\ (P^- \omega - \omega)(x_{i+\frac{1}{2}}, y_{j+\frac{1}{2}}) &= 0, \end{aligned}$$

where $P^k(D)$ represents the polynomials of degree k over the interval D . Furthermore, we also define Π_x^+ and Π_y^+ onto χ_h [5]: for each cell K ,

$$\begin{aligned} (\Pi_x^+ \omega - \omega, \vartheta_x)_K &= 0, & \forall \vartheta \in Q^k(K), \\ \int_{J_j} (\Pi_x^+ \omega - \omega)(x_{i-\frac{1}{2}}, y) \vartheta(y) dy &= 0, & \forall \vartheta \in P^k(J_j), \\ (\Pi_y^+ \omega - \omega, \vartheta_y)_K &= 0, & \forall \vartheta \in Q^k(K), \\ \int_{I_i} (\Pi_y^+ \omega - \omega)(x, y_{j-\frac{1}{2}}) \vartheta(x) dx &= 0, & \forall \vartheta \in P^k(I_i), \end{aligned}$$

as well as a vector-valued projection

$$\mathbf{\Pi}^+ \begin{pmatrix} s_1 \\ s_2 \end{pmatrix} = \begin{pmatrix} \Pi_x^+ s_1 \\ \Pi_y^+ s_2 \end{pmatrix}.$$

Based on the above definitions, we can similarly define the projections $\underline{\mathbf{\Pi}}^+$ and \mathbf{P}^- . For the vector-valued function $\mathbf{p} = (p_1, p_2)^\top \in \mathbf{M}$, we define

$$\mathbf{P}^- \mathbf{p} = (P^- p_1, P^- p_2)^\top.$$

For the matrix-valued function $\underline{w} = (\mathbf{w}_1, \mathbf{w}_2) \in \underline{\omega}$, we define \mathbf{w}_1 and \mathbf{w}_2 as its two column vectors,

$$\underline{\mathbf{\Pi}}^+ \underline{w} = (\mathbf{\Pi}^+ \mathbf{w}_1, \mathbf{\Pi}^+ \mathbf{w}_2).$$

In addition, the following definitions are given

$$(\omega, \vartheta) = \sum_{K \in \Omega_h} (\omega, \vartheta)_K, \quad (\boldsymbol{\omega}, \boldsymbol{\vartheta}) = \sum_{K \in \Omega_h} (\boldsymbol{\omega}, \boldsymbol{\vartheta})_K, \quad (\underline{\omega} : \underline{\vartheta}) = \sum_{K \in \Omega_h} (\underline{\omega} : \underline{\vartheta})_K,$$

where

$$(\omega, \vartheta)_K = \int_K \omega \vartheta dx dy, \quad (\boldsymbol{\omega}, \boldsymbol{\vartheta})_K = \int_K \boldsymbol{\omega} \cdot \boldsymbol{\vartheta} dx dy, \quad (\underline{\omega} : \underline{\vartheta})_K = \int_K \underline{\omega} : \underline{\vartheta} dx dy.$$

Moreover, we define

$$\underline{\omega} : \underline{r} = \sum_{i,j=1}^d \omega_{ij} r_{ij}, \quad \mathbf{v} \cdot \underline{\omega} \cdot \mathbf{n} = \sum_{i,j=1}^d \mathbf{v}_i \omega_{ij} \mathbf{n}_j.$$

The error of the projections is given by the following lemma [5].

Lemma 2.2. For arbitrary projection P_h , which is either P^- , Π_x^+ or Π_y^+ , and $q \in H^{k+1}(\Omega)$, we have

$$\|q - P_h q\| + h^{1/2} \|q - P_h q\|_{\Gamma_h} \leq Ch^{k+1}.$$

Next, we give the following lemma which has been demonstrated in [12].

Lemma 2.3. Let $q \in C^{k+1}(\Omega)$ and $\Pi q \in \chi_h$. We assume that $\|q - \Pi q\| \leq Ch^{\tilde{\kappa}}$ for some constant $C > 0$ independent of h and $\tilde{\kappa} \leq k + 1$, then there holds

$$h \|q - \Pi q\|_{\infty} + h^{1/2} \|q - \Pi q\|_{\Gamma_h} \leq Ch^{\tilde{\kappa}}.$$

Additionally, we give the following superconvergence property [6].

Lemma 2.4. We assume $q \in H^{k+2}(\Omega)$, then for arbitrary cell K and $\mathbf{v} \in \mathbf{M}_h$, we have

$$|(q - P^- q, \nabla \cdot \mathbf{v})_K - \langle q - P^- q, \mathbf{v} \cdot \mathbf{n}_K \rangle_{\partial K}| \leq Ch^{k+1} \|q\|_{k+2} \|\mathbf{v}\|_K,$$

where the projection P^- is defined on the Cartesian meshes, \mathbf{n}_K is the outward normal, and $C > 0$ is a constant independent of K and h .

3 IMEX-LDG schemes

Two fully-discrete LDG schemes are given in this section. We first construct the semi-discrete scheme.

3.1 Semi-discrete LDG Scheme

By introducing auxiliary variables \mathbf{q} , \mathbf{u} , \underline{w} , we rewrite (1.1a)-(1.1c) into

$$\frac{\partial \rho}{\partial t} = -\nabla \cdot \mathbf{q} + g\rho(1-\rho), \tag{3.1a}$$

$$\mathbf{q} = \rho \mathbf{p} - \nabla \rho, \tag{3.1b}$$

$$\frac{\partial c}{\partial t} = \nabla \cdot \mathbf{u} + \rho - c, \tag{3.1c}$$

$$\frac{1}{D_c} \mathbf{u} = \nabla c + \frac{\kappa}{D_c} \rho \mathbf{p}, \tag{3.1d}$$

$$\frac{\partial \mathbf{p}}{\partial t} = -\Gamma \mathbf{p} + \nabla \cdot \underline{w} + S \nabla c - \Gamma_2 |\mathbf{p}|^2 \mathbf{p}, \tag{3.1e}$$

$$\underline{w} = D_p \nabla \mathbf{p}. \tag{3.1f}$$

The LDG scheme of (3.1a)-(3.1f) is to find $\rho_h, c_h \in \chi_h, \mathbf{q}_h, \mathbf{p}_h, \mathbf{u}_h \in \mathbf{M}_h, \underline{w}_h \in \underline{\omega}_h$, such that for arbitrary $v, \zeta, \boldsymbol{\alpha}, \boldsymbol{\beta}, \boldsymbol{\theta}, \underline{r} \in \chi_h \times \chi_h \times \mathbf{M}_h \times \mathbf{M}_h \times \mathbf{M}_h \times \underline{\omega}_h$, we have

$$\left(\frac{\partial \rho_h}{\partial t}, v\right)_K = \mathcal{H}_K(\mathbf{q}_h, v) + (g\rho_h(1-\rho_h), v)_K, \tag{3.2a}$$

$$(\mathbf{q}_h, \boldsymbol{\alpha})_K = (\rho_h \mathbf{p}_h, \boldsymbol{\alpha})_K + \mathcal{D}_K(\rho_h, \boldsymbol{\alpha}), \tag{3.2b}$$

$$\left(\frac{\partial c_h}{\partial t}, \zeta\right)_K = -\mathcal{H}_K(\mathbf{u}_h, \zeta) + (\rho_h, \zeta)_K - (c_h, \zeta)_K, \tag{3.2c}$$

$$\left(\frac{1}{\mathcal{D}_c} \mathbf{u}_h, \boldsymbol{\theta}\right)_K = -\mathcal{D}_K(c_h, \boldsymbol{\theta}) + \frac{\kappa}{\mathcal{D}_c} (\rho_h \mathbf{p}_h, \boldsymbol{\theta})_K, \tag{3.2d}$$

$$\left(\frac{\partial \mathbf{p}_h}{\partial t}, \boldsymbol{\beta}\right)_K = -\mathcal{L}_K(\underline{w}_h, \boldsymbol{\beta}) + (-\Gamma \mathbf{p}_h - \Gamma_2 |\mathbf{p}_h|^2 \mathbf{p}_h, \boldsymbol{\beta})_K - S \mathcal{D}_K(c_h, \boldsymbol{\beta}), \tag{3.2e}$$

$$\left(\frac{1}{\mathcal{D}_p} \underline{w}_h : \underline{r}\right)_K = -\mathcal{K}_K(\mathbf{p}_h, \underline{r}), \tag{3.2f}$$

where

$$\begin{aligned} \mathcal{H}_K(\mathbf{q}_h, v) &= (\mathbf{q}_h, \nabla v)_K - \langle \widehat{\mathbf{q}}_h \cdot \mathbf{n}_K, v \rangle_{\partial K}, & \mathcal{D}_K(\rho_h, \boldsymbol{\alpha}) &= (\rho_h, \nabla \cdot \boldsymbol{\alpha})_K - \langle \widehat{\rho}_h, \boldsymbol{\alpha} \cdot \mathbf{n}_K \rangle_{\partial K}, \\ \mathcal{L}_K(\underline{w}_h, \boldsymbol{\beta}) &= (\underline{w}_h : \nabla \boldsymbol{\beta})_K - \langle \widehat{\underline{w}}_h \cdot \mathbf{n}_K, \boldsymbol{\beta} \rangle_{\partial K}, & \mathcal{K}_K(\mathbf{p}_h, \underline{r}) &= (\mathbf{p}_h, \nabla \cdot \underline{r})_K - \langle \widehat{\mathbf{p}}_h, \underline{r} \cdot \mathbf{n}_K \rangle_{\partial K}. \end{aligned}$$

Moreover, we define

$$\Xi(\cdot, \cdot) = \sum_{K \in \Omega_h} \Xi_K(\cdot, \cdot) \quad \text{with } \Xi = \mathcal{H}, \mathcal{D}, \mathcal{L}, \mathcal{K}.$$

Alternating numerical fluxes are chosen as

$$\widehat{\mathbf{q}}_h = \mathbf{q}_h^+, \quad \widehat{\rho}_h = \rho_h^-, \quad \widehat{\mathbf{u}}_h = \mathbf{u}_h^+, \quad \widehat{c}_h = c_h^-, \tag{3.2d}, \quad \widehat{\underline{w}}_h = \underline{w}_h^+, \quad \widehat{\mathbf{p}}_h = \mathbf{p}_h^-.$$

Specifically, in equation (3.2e), the choice of numerical flux \widehat{c}_h depends on the sign of the coefficient S , if S is positive, $\widehat{c}_h = c_h^-$, if S is negative, $\widehat{c}_h = c_h^+$. The following identification may be easily verified by integration by parts.

Lemma 3.1. For arbitrary $(v, \mathbf{q}, \mathbf{u}, \underline{w}) \in \chi_h \times \mathbf{M}_h \times \mathbf{M}_h \times \underline{\omega}_h$, there hold

$$\mathcal{H}(\mathbf{q}, v) + \mathcal{D}(v, \mathbf{q}) = 0, \quad \mathcal{L}(\underline{w}, \mathbf{u}) + \mathcal{K}(\mathbf{u}, \underline{w}) = 0. \tag{3.3}$$

3.2 Fully-discrete LDG scheme

Dividing the time interval $[0, T]$ uniformly into M parts, with $\tau = T/M$ representing the time step, we consider two IMEX time integrations with LDG spatial discretization.

3.2.1 IMEX-LDG($k,1$) scheme

We consider IMEX-LDG($k,1$) as the first-order time integration indicated as below. For any $n \geq 0$, we assume the numerical solutions $\rho_h^n, c_h^n, \mathbf{p}_h^n, \mathbf{q}_h^n, \mathbf{u}_h^n, \underline{w}_h^n$ are known, then we calculate the numerical solutions $\rho_h^{n+1}, \mathbf{q}_h^{n+1}$ by

$$\left(\frac{\rho_h^{n+1} - \rho_h^n}{\tau}, v\right) = \mathcal{H}(\mathbf{q}_h^{n+1}, v) + (g\rho_h^{n+1}(1 - \rho_h^n), v), \tag{3.4a}$$

$$(\mathbf{q}_h^{n+1}, \boldsymbol{\alpha}) = (\rho_h^{n+1} \mathbf{p}_h^n, \boldsymbol{\alpha}) + \mathcal{D}(\rho_h^{n+1}, \boldsymbol{\alpha}), \tag{3.4b}$$

for any $v \in \chi_h, \boldsymbol{\alpha} \in \mathbf{M}_h$. After that, we find the numerical solutions $c_h^{n+1}, \mathbf{u}_h^{n+1}$ by

$$\left(\frac{c_h^{n+1} - c_h^n}{\tau}, \zeta\right) = -\mathcal{H}(\mathbf{u}_h^{n+1}, \zeta) + (\rho_h^{n+1}, \zeta) - (c_h^{n+1}, \zeta), \tag{3.5a}$$

$$\left(\frac{1}{\mathcal{D}_c} \mathbf{u}_h^{n+1}, \boldsymbol{\theta}\right) = \left(\frac{\kappa}{\mathcal{D}_c} \rho_h^{n+1} \mathbf{p}_h^n, \boldsymbol{\theta}\right) - \mathcal{D}(c_h^{n+1}, \boldsymbol{\theta}), \tag{3.5b}$$

for any $\zeta \in \chi_h, \boldsymbol{\theta} \in \mathbf{M}_h$. Finally, we compute the numerical solutions $\mathbf{p}_h^{n+1}, \underline{w}_h^{n+1}$ by

$$\left(\frac{\mathbf{p}_h^{n+1} - \mathbf{p}_h^n}{\tau}, \boldsymbol{\beta}\right) = -\mathcal{L}(\underline{w}_h^{n+1}, \boldsymbol{\beta}) + (-\Gamma \mathbf{p}_h^{n+1} - \Gamma_2 |\mathbf{p}_h^{n+1}|^2 \mathbf{p}_h^{n+1}, \boldsymbol{\beta}) - \mathcal{SD}(c_h^{n+1}, \boldsymbol{\beta}), \tag{3.6a}$$

$$\left(\frac{1}{\mathcal{D}_p} \underline{w}_h^{n+1}, r\right) = -\mathcal{K}(\mathbf{p}_h^{n+1}, r), \tag{3.6b}$$

for any $\boldsymbol{\beta} \in \mathbf{M}_h, r \in \omega_h$. To start this scheme, we provide the initial conditions through projections:

$$\rho_h^0 = P^- \rho_0, \quad c_h^0 = P^- c_0, \quad \mathbf{p}_h^0 = \mathbf{P}^- \mathbf{p}_0. \tag{3.7}$$

3.2.2 IMEX-LDG($k,2$) scheme

We consider IMEX-LDG($k,2$) as the second-order time integration indicated as below. For any $n \geq 1$, we assume the numerical solutions at t^n, t^{n-1} are known, then we calculate the numerical solutions $\rho_h^{n+1}, \mathbf{q}_h^{n+1}$ by

$$\left(\frac{\rho_h^{n+1} - \rho_h^n}{\tau}, v\right) = \mathcal{H}\left(\frac{\mathbf{q}_h^{n+1} + \mathbf{q}_h^n}{2}, v\right) + \left(g\rho_h^{n+\frac{1}{2}} \left(1 - \frac{3\rho_h^n - \rho_h^{n-1}}{2}\right), v\right), \tag{3.8a}$$

$$\left(\frac{\mathbf{q}_h^{n+1} + \mathbf{q}_h^n}{2}, \boldsymbol{\alpha}\right) = \left(\rho_h^{n+\frac{1}{2}} \frac{3\mathbf{p}_h^n - \mathbf{p}_h^{n-1}}{2}, \boldsymbol{\alpha}\right) + \mathcal{D}\left(\frac{\rho_h^{n+1} + \rho_h^n}{2}, \boldsymbol{\alpha}\right), \tag{3.8b}$$

for any $v \in \chi_h, \boldsymbol{\alpha} \in \mathbf{M}_h$. After that, we calculate the numerical solutions $c_h^{n+1}, \mathbf{u}_h^{n+1}$ by

$$\left(\frac{c_h^{n+1} - c_h^n}{\tau}, \zeta\right) = -\mathcal{H}\left(\frac{\mathbf{u}_h^{n+1} + \mathbf{u}_h^n}{2}, \zeta\right) + \left(\frac{\rho_h^{n+1} + \rho_h^n}{2}, \zeta\right) - \left(\frac{c_h^{n+1} + c_h^n}{2}, \zeta\right), \tag{3.9a}$$

$$\left(\frac{1}{\mathcal{D}_c} \frac{\mathbf{u}_h^{n+1} + \mathbf{u}_h^n}{2}, \boldsymbol{\theta}\right) = \left(\frac{\kappa}{\mathcal{D}_c} \rho_h^{n+\frac{1}{2}} \frac{3\mathbf{p}_h^n - \mathbf{p}_h^{n-1}}{2}, \boldsymbol{\theta}\right) - \mathcal{D}\left(\frac{c_h^{n+1} + c_h^n}{2}, \boldsymbol{\theta}\right), \tag{3.9b}$$

for any $\zeta \in \chi_h, \theta \in \mathbf{M}_h$. Finally, we find the numerical solutions $\mathbf{p}_h^{n+1}, \underline{w}_h^{n+1}$ by

$$\begin{aligned} \left(\frac{\mathbf{p}_h^{n+1} - \mathbf{p}_h^n}{\tau}, \beta\right) &= -\mathcal{L}\left(\frac{\underline{w}_h^{n+1} + \underline{w}_h^n}{2}, \beta\right) + \left(-\Gamma \frac{\mathbf{p}_h^{n+1} + \mathbf{p}_h^n}{2} - \Gamma_2 \left|\frac{3\mathbf{p}_h^n - \mathbf{p}_h^{n-1}}{2}\right|^2 \mathbf{p}_h^{n+\frac{1}{2}}, \beta\right) \\ &\quad - S\mathcal{D}\left(\frac{c_h^{n+1} + c_h^n}{2}, \beta\right), \end{aligned} \tag{3.10a}$$

$$\left(\frac{1}{D_p} \frac{\underline{w}_h^{n+1} + \underline{w}_h^n}{2}; r\right) = -\mathcal{K}\left(\frac{\mathbf{p}_h^{n+1} + \mathbf{p}_h^n}{2}, r\right), \tag{3.10b}$$

for any $\beta \in \mathbf{M}_h, r \in \underline{\omega}_h$, where

$$\rho_h^{n+\frac{1}{2}} = \frac{\rho_h^n + \rho_h^{n+1}}{2}, \quad \mathbf{p}_h^{n+\frac{1}{2}} = \frac{\mathbf{p}_h^n + \mathbf{p}_h^{n+1}}{2}.$$

To avoid time level mismatch of the spatial discretization, the schemes (3.8b), (3.9b) and (3.10b) are symmetric about $t^{n+\frac{1}{2}}$. Moreover, we can linearize the scheme using the extrapolation in absolute value in (3.10a).

To start this scheme, the initial conditions at time levels t^0 and t^1 are needed. The solutions at t^0 are obtained from (3.7), and the solutions at t^1 are taken from the IMEX-LDG($k,1$) scheme in Subsection 3.2.1.

4 Error estimate

We denote e as the error between the exact and numerical solutions throughout this paper, i.e.,

$$e_\rho = \rho - \rho_h, \quad \mathbf{e}_q = \mathbf{q} - \mathbf{q}_h, \quad e_c = c - c_h, \quad \mathbf{e}_u = \mathbf{u} - \mathbf{u}_h, \quad \mathbf{e}_p = \mathbf{p} - \mathbf{p}_h, \quad \underline{e}_w = \underline{w} - \underline{w}_h.$$

We split the errors into two terms as follows

$$\begin{aligned} e_\rho &= \tilde{\zeta}_\rho - \eta_\rho, & \eta_\rho &= P^- \rho - \rho, & \tilde{\zeta}_\rho &= P^- \rho - \rho_h, \\ \mathbf{e}_q &= \tilde{\zeta}_q - \eta_q, & \eta_q &= \Pi^+ \mathbf{q} - \mathbf{q}, & \tilde{\zeta}_q &= \Pi^+ \mathbf{q} - \mathbf{q}_h, \\ e_c &= \tilde{\zeta}_c - \eta_c, & \eta_c &= P^- c - c, & \tilde{\zeta}_c &= P^- c - c_h, \\ \mathbf{e}_u &= \tilde{\zeta}_u - \eta_u, & \eta_u &= \Pi^+ \mathbf{u} - \mathbf{u}, & \tilde{\zeta}_u &= \Pi^+ \mathbf{u} - \mathbf{u}_h, \\ \mathbf{e}_p &= \tilde{\zeta}_p - \eta_p, & \eta_p &= \mathbf{P}^- \mathbf{p} - \mathbf{p}, & \tilde{\zeta}_p &= \mathbf{P}^- \mathbf{p} - \mathbf{p}_h, \\ \underline{e}_w &= \tilde{\zeta}_{\underline{w}} - \eta_{\underline{w}}, & \eta_{\underline{w}} &= \Pi^+ \underline{w} - \underline{w}, & \tilde{\zeta}_{\underline{w}} &= \Pi^+ \underline{w} - \underline{w}_h. \end{aligned}$$

Then we can easily prove that

$$\mathcal{H}(\eta_u, \sigma) = \mathcal{H}(\eta_q, \sigma) = 0, \quad \mathcal{L}(\eta_{\underline{w}}, \sigma) = 0, \quad \forall \sigma \in Q^k(K). \tag{4.1}$$

Following [17], the following properties hold by Lemma 2.2 and the linear structure of elliptic projection.

Lemma 4.1. For any $n \geq 0$, we have

$$\|\boldsymbol{\eta}_p^n\| + \|\eta_\rho^n\| + \|\eta_c^n\| + \|\boldsymbol{\eta}_q^n\| + \|\boldsymbol{\eta}_u^n\| + \|\underline{\eta}_{\underline{w}}^n\| \leq Ch^{k+1}, \tag{4.2a}$$

$$\|\boldsymbol{\eta}_p^n\|_\infty + \|\eta_\rho^n\|_\infty + \|\eta_c^n\|_\infty + \|\boldsymbol{\eta}_q^n\|_\infty + \|\boldsymbol{\eta}_u^n\|_\infty + \|\underline{\eta}_{\underline{w}}^n\|_\infty \leq Ch^k, \tag{4.2b}$$

$$\|\eta_\rho^{n+1} - \eta_\rho^n\| + \|\eta_c^{n+1} - \eta_c^n\| + \|\boldsymbol{\eta}_p^{n+1} - \boldsymbol{\eta}_p^n\| \leq Ch^{k+1}\tau. \tag{4.2c}$$

Then there hold the following initial results by (3.7)

$$\xi_\rho^0 = P^- \rho_0 - \rho_h^0 = 0, \quad \xi_c^0 = P^- c_0 - c_h^0 = 0, \quad \xi_p^0 = \mathbf{P}^- \mathbf{p}_0 - \mathbf{p}_h^0 = 0. \tag{4.3}$$

Refer to [17–20] with certain minor changes, we will obtain the following important relationship, so we omit the detailed proof here.

Lemma 4.2. Assume that ξ_p and $\xi_{\underline{w}}$ are defined above. We have

$$\|\nabla \xi_p\| \leq C(\|\xi_{\underline{w}}\| + h^{k+1}), \quad h^{-\frac{1}{2}}\|\xi_p\|_{\Gamma_h} \leq C(\|\xi_{\underline{w}}\| + h^{k+1}).$$

Then we follow [21] and give a priori hypothesis that

$$\|\mathbf{e}_p^m\| + \|e_\rho^m\| \leq h^{1+\delta}, \quad 0 \leq m \leq n, \tag{4.4}$$

where h is small enough and δ is any given positive constant, which further implies

$$\|\mathbf{p}_h^m\|_\infty + \|\rho_h^m\|_\infty \leq C, \quad 0 \leq m \leq n, \tag{4.5}$$

by hypothesis 3 and Lemma 2.3. The above a priori assumption will be proved in Section 4.2.

Next, we state the error estimate of the IMEX-LDG($k,1$) scheme.

4.1 The proof of the IMEX-LDG($k,1$) scheme

Theorem 4.1. Suppose the exact solutions of the problem (3.1a)-(3.1f) satisfy $\rho \in L^\infty(0, T; H^{k+3})$, $\mathbf{q} \in L^\infty(0, T; (H^{k+2})^2)$, $c \in L^\infty(0, T; H^{k+3})$, $\mathbf{u} \in L^\infty(0, T; (H^{k+2})^2)$, $\underline{w} \in L^\infty(0, T; (H^{k+2})^{2 \times 2})$ and $\mathbf{p} \in L^\infty(0, T; (H^{k+3})^2)$. The exact solutions are second-order differentiable. The numerical solutions of IMEX-LDG($k,1$) are $\rho_h, \mathbf{q}_h, c_h, \mathbf{u}_h, \mathbf{p}_h, \underline{w}_h$, which satisfy the initial condition (3.7). If the finite element space is the piecewise tensor product polynomials of degree up to k , suppose $C\tau \leq \frac{1}{2}$ and the temporal-spatial condition $\tau \leq h^{1+\frac{3\delta}{2}}$, where $\delta \leq \frac{2}{3}k$, ($k \geq 1$) is given constant, then the error estimate of IMEX-LDG($k,1$) scheme is obtained

$$\begin{aligned} & \|e_\rho^n\|^2 + \|e_c^n\|^2 + \|\mathbf{e}_p^n\|^2 + \tau \sum_{m=1}^n \|\mathbf{e}_q^m\|^2 + \tau \sum_{m=1}^n \|\mathbf{e}_u^m\|^2 + \tau \sum_{m=1}^n \|\underline{e}_{\underline{w}}^m\|^2 \\ & \leq C(h^{2k+2} + \tau^2), \quad \forall n \geq 1. \end{aligned}$$

The first-order time marching scheme is considered in this section. For any $n \geq 0$, we have the following equations about the exact solutions

$$\left(\frac{\rho^{n+1}-\rho^n}{\tau}, v\right) = \mathcal{H}(\mathbf{q}^{n+1}, v) + (g\rho^{n+1}(1-\rho^n), v) + (\zeta_1^n, v), \tag{4.6a}$$

$$(\mathbf{q}^{n+1}, \boldsymbol{\alpha}) = (\rho^{n+1}\mathbf{p}^n, \boldsymbol{\alpha}) + \mathcal{D}(\rho^{n+1}, \boldsymbol{\alpha}) + (\zeta_2^n, \boldsymbol{\alpha}), \tag{4.6b}$$

$$\left(\frac{c^{n+1}-c^n}{\tau}, \zeta\right) = -\mathcal{H}(\mathbf{u}^{n+1}, \zeta) + (\rho^{n+1}, \zeta) - (c^{n+1}, \zeta) + (\zeta_3^n, \zeta), \tag{4.6c}$$

$$\left(\frac{1}{\mathcal{D}_c}\mathbf{u}^{n+1}, \boldsymbol{\theta}\right) = \left(\frac{\kappa}{\mathcal{D}_c}\rho^{n+1}\mathbf{p}^n, \boldsymbol{\theta}\right) - \mathcal{D}(c^{n+1}, \boldsymbol{\theta}) + (\zeta_4^n, \boldsymbol{\theta}), \tag{4.6d}$$

$$\begin{aligned} \left(\frac{\mathbf{p}^{n+1}-\mathbf{p}^n}{\tau}, \boldsymbol{\beta}\right) &= -\mathcal{L}(\underline{w}^{n+1}, \boldsymbol{\beta}) - (\Gamma\mathbf{p}^{n+1}, \boldsymbol{\beta}) - (\Gamma_2|\mathbf{p}^n|^2\mathbf{p}^{n+1}, \boldsymbol{\beta}) \\ &\quad - S\mathcal{D}(c^{n+1}, \boldsymbol{\beta}) + (\zeta_5^n, \boldsymbol{\beta}), \end{aligned} \tag{4.6e}$$

$$\left(\frac{1}{\mathcal{D}_p}\underline{w}^{n+1}; \underline{r}\right) = -\mathcal{K}(\mathbf{p}^{n+1}, \underline{r}). \tag{4.6f}$$

Here local truncation errors ζ_i^n , ($i = 1, \dots, 5$) satisfy

$$\|\zeta_i^n\| \leq C\tau, \quad i = 1, \dots, 5, \quad \forall n \geq 0. \tag{4.7}$$

Subtracting (4.6a)-(4.6f) from (3.4a)-(3.6b), the following error equations are given

$$\left(\frac{e_\rho^{n+1}-e_\rho^n}{\tau}, v\right) = \mathcal{H}(\mathbf{e}_q^{n+1}, v) + (g\rho^{n+1}(1-\rho^n) - g\rho_h^{n+1}(1-\rho_h^n), v) + (\zeta_1^n, v), \tag{4.8a}$$

$$(\mathbf{e}_q^{n+1}, \boldsymbol{\alpha}) = (\rho^{n+1}\mathbf{p}^n, \boldsymbol{\alpha}) - (\rho_h^{n+1}\mathbf{p}_h^n, \boldsymbol{\alpha}) + \mathcal{D}(e_\rho^{n+1}, \boldsymbol{\alpha}) + (\zeta_2^n, \boldsymbol{\alpha}), \tag{4.8b}$$

$$\left(\frac{e_c^{n+1}-e_c^n}{\tau}, \zeta\right) = -\mathcal{H}(\mathbf{e}_u^{n+1}, \zeta) + (e_\rho^{n+1}, \zeta) - (e_c^{n+1}, \zeta) + (\zeta_3^n, \zeta), \tag{4.8c}$$

$$\left(\frac{1}{\mathcal{D}_c}\mathbf{e}_u^{n+1}, \boldsymbol{\theta}\right) = \frac{\kappa}{\mathcal{D}_c}(\rho^{n+1}\mathbf{p}^n - \rho_h^{n+1}\mathbf{p}_h^n, \boldsymbol{\theta}) - \mathcal{D}(e_c^{n+1}, \boldsymbol{\theta}) + (\zeta_4^n, \boldsymbol{\theta}), \tag{4.8d}$$

$$\begin{aligned} \left(\frac{\mathbf{e}_p^{n+1}-\mathbf{e}_p^n}{\tau}, \boldsymbol{\beta}\right) &= -\mathcal{L}(\underline{e}_w^{n+1}, \boldsymbol{\beta}) - (\Gamma\mathbf{e}_p^{n+1}, \boldsymbol{\beta}) - (\Gamma_2|\mathbf{p}^n|^2\mathbf{p}^{n+1}, \boldsymbol{\beta}) + (\Gamma_2|\mathbf{p}_h^n|^2\mathbf{p}_h^{n+1}, \boldsymbol{\beta}) \\ &\quad - S\mathcal{D}(e_c^{n+1}, \boldsymbol{\beta}) + (\zeta_5^n, \boldsymbol{\beta}), \end{aligned} \tag{4.8e}$$

$$\left(\frac{1}{\mathcal{D}_p}\underline{e}_w^{n+1}; \underline{r}\right) = -\mathcal{K}(\mathbf{e}_p^{n+1}, \underline{r}). \tag{4.8f}$$

Proof. By using the Schwarz inequality, Lemma 2.4, Lemma 3.1, Lemma 4.1, (4.5), (4.3), (4.1), Lemma 4.2 and hypotheses, we take $v = \zeta_\rho^{n+1}$ in (4.8a), $\boldsymbol{\alpha} = \zeta_q^{n+1}$ in (4.8b), $\zeta = \zeta_c^{n+1}$ in (4.8c), $\boldsymbol{\theta} = \zeta_u^{n+1}$ in (4.8d), $\boldsymbol{\beta} = \zeta_p^{n+1}$ in (4.8e) and $\underline{r} = \zeta_w^{n+1}$ in (4.8f), and sum up these

equations to get

$$\begin{aligned} & \|\xi_\rho^n\|^2 + \|\xi_c^n\|^2 + \|\xi_p^n\|^2 + \tau \sum_{m=1}^n \|\xi_q^m\|^2 + \tau \sum_{m=1}^n \|\xi_u^m\|^2 + \tau \sum_{m=1}^n \|\xi_w^m\|^2 \\ & \leq C(h^{2k+2} + \tau^2), \quad \forall n \geq 1, \end{aligned} \tag{4.9}$$

where we use the discrete Gronwall’s inequality, which further derive the above theorem. For more details, it is easy to be deduced, we omit it here. Next we mainly focus on the proof of the IMEX-LDG($k,2$) scheme. \square

4.2 The proof of the IMEX-LDG($k,2$) scheme

Theorem 4.2. *Suppose the exact solutions of the problem (3.1a)-(3.1f) satisfy $\rho \in L^\infty(0, T; H^{k+3})$, $\mathbf{q} \in L^\infty(0, T; (H^{k+2})^2)$, $c \in L^\infty(0, T; H^{k+3})$, $\mathbf{u} \in L^\infty(0, T; (H^{k+2})^2)$, $w \in L^\infty(0, T; (H^{k+2})^{2 \times 2})$ and $\mathbf{p} \in L^\infty(0, T; (H^{k+3})^2)$. The exact solutions are third-order differentiable. The numerical solutions of IMEX-LDG($k,2$) are $\rho_h, c_h, \mathbf{p}_h, \mathbf{q}_h, \mathbf{u}_h, w_h$ which satisfy the initial condition (3.7). If the finite element space is the piecewise tensor product polynomials of degree up to k , suppose $C\tau \leq \frac{1}{4}$ and the temporal-spatial condition $\tau \leq h^{\frac{1}{2} + \frac{3\delta}{4}}$, where $\delta \leq \frac{2}{3}k$ ($k \geq 1$) is given constant. Then the error estimate of IMEX-LDG($k,2$) scheme is obtained*

$$\begin{aligned} & \|e_\rho^n\|^2 + \|e_c^n\|^2 + \|e_p^n\|^2 + \tau \sum_{m=2}^n \left\| \frac{\mathbf{e}_q^m + \mathbf{e}_q^{m-1}}{2} \right\|^2 + \tau \sum_{m=2}^n \left\| \frac{\mathbf{e}_u^m + \mathbf{e}_u^{m-1}}{2} \right\|^2 \\ & + \tau \sum_{m=2}^n \left\| \frac{e_w^m + e_w^{m-1}}{2} \right\|^2 \leq C(h^{2k+2} + \tau^4), \quad \forall n \geq 2. \end{aligned}$$

For any $n \geq 1$, we have the following equations about the exact solutions

$$\left(\frac{\rho^{n+1} - \rho^n}{\tau}, v \right) = \mathcal{H} \left(\frac{\mathbf{q}^{n+1} + \mathbf{q}^n}{2}, v \right) + \left(g\rho^{n+\frac{1}{2}} \left(1 - \frac{3\rho^n - \rho^{n-1}}{2} \right), v \right) + (\zeta_1^{n+\frac{1}{2}}, v), \tag{4.10a}$$

$$\left(\frac{\mathbf{q}^{n+1} + \mathbf{q}^n}{2}, \alpha \right) = \left(\rho^{n+\frac{1}{2}} \frac{3\mathbf{p}^n - \mathbf{p}^{n-1}}{2}, \alpha \right) + \mathcal{D} \left(\frac{\rho^{n+1} + \rho^n}{2}, \alpha \right) + (\zeta_2^{n+\frac{1}{2}}, \alpha), \tag{4.10b}$$

$$\left(\frac{c^{n+1} - c^n}{\tau}, \zeta \right) = -\mathcal{H} \left(\frac{\mathbf{u}^{n+1} + \mathbf{u}^n}{2}, \zeta \right) + \left(\frac{\rho^{n+1} + \rho^n}{2}, \zeta \right) - \left(\frac{c^{n+1} + c^n}{2}, \zeta \right) + (\zeta_3^{n+\frac{1}{2}}, \zeta), \tag{4.10c}$$

$$\left(\frac{1}{\mathcal{D}_c} \frac{\mathbf{u}^{n+1} + \mathbf{u}^n}{2}, \theta \right) = \left(\frac{\kappa}{\mathcal{D}_c} \rho^{n+\frac{1}{2}} \frac{3\mathbf{p}^n - \mathbf{p}^{n-1}}{2}, \theta \right) - \mathcal{D} \left(\frac{c^{n+1} + c^n}{2}, \theta \right) + (\zeta_4^{n+\frac{1}{2}}, \theta), \tag{4.10d}$$

$$\begin{aligned} \left(\frac{\mathbf{p}^{n+1} - \mathbf{p}^n}{\tau}, \beta \right) &= -\mathcal{L} \left(\frac{w^{n+1} + w^n}{2}, \beta \right) + \left(-\Gamma \mathbf{p}^{n+\frac{1}{2}} - \Gamma_2 \left| \frac{3\mathbf{p}^n - \mathbf{p}^{n-1}}{2} \right|^2 \mathbf{p}^{n+\frac{1}{2}}, \beta \right) \\ &\quad - S\mathcal{D} \left(\frac{c^{n+1} + c^n}{2}, \beta \right) + (\zeta_5^{n+\frac{1}{2}}, \beta), \end{aligned} \tag{4.10e}$$

$$\left(\frac{1}{\mathcal{D}_p} \frac{w^{n+1} + w^n}{2}, r \right) = -\mathcal{K}(\mathbf{p}^{n+\frac{1}{2}}, r). \tag{4.10f}$$

Here $\zeta_i^{n+\frac{1}{2}}, (i=1, \dots, 5)$ satisfy

$$\left\| \zeta_i^{n+\frac{1}{2}} \right\| \leq C\tau^2, \quad n \geq 1. \tag{4.11}$$

Subtracting (4.10a)-(4.10f) from (3.8a)-(3.10b), the following error equations are given

$$\begin{aligned} \left(\frac{e_\rho^{n+1} - e_\rho^n}{\tau}, v \right) &= \mathcal{H} \left(\frac{\mathbf{e}_q^{n+1} + \mathbf{e}_q^n}{2}, v \right) + \left(g\rho^{n+\frac{1}{2}} \left(1 - \frac{3\rho^n - \rho^{n-1}}{2} \right), v \right) \\ &\quad - \left(g\rho_h^{n+\frac{1}{2}} \left(1 - \frac{3\rho_h^n - \rho_h^{n-1}}{2} \right), v \right) + (\zeta_1^{n+\frac{1}{2}}, v), \end{aligned} \tag{4.12a}$$

$$\begin{aligned} \left(\frac{\mathbf{e}_q^{n+1} + \mathbf{e}_q^n}{2}, \alpha \right) &= \left(\rho^{n+\frac{1}{2}} \frac{3\mathbf{p}^n - \mathbf{p}^{n-1}}{2}, \alpha \right) - \left(\rho_h^{n+\frac{1}{2}} \frac{3\mathbf{p}_h^n - \mathbf{p}_h^{n-1}}{2}, \alpha \right) \\ &\quad + \mathcal{D} \left(\frac{e_\rho^{n+1} + e_\rho^n}{2}, \alpha \right) + (\zeta_2^{n+\frac{1}{2}}, \alpha), \end{aligned} \tag{4.12b}$$

$$\left(\frac{e_c^{n+1} - e_c^n}{\tau}, \zeta \right) = -\mathcal{H} \left(\frac{\mathbf{e}_u^{n+1} + \mathbf{e}_u^n}{2}, \zeta \right) + \left(\frac{e_\rho^{n+1} + e_\rho^n}{2}, \zeta \right) - \left(\frac{e_c^{n+1} + e_c^n}{2}, \zeta \right) + (\zeta_3^{n+\frac{1}{2}}, \zeta), \tag{4.12c}$$

$$\begin{aligned} \left(\frac{1}{\mathcal{D}_c} \frac{\mathbf{e}_u^{n+1} + \mathbf{e}_u^n}{2}, \theta \right) &= \left(\frac{\kappa}{\mathcal{D}_c} \rho^{n+\frac{1}{2}} \frac{3\mathbf{p}^n - \mathbf{p}^{n-1}}{2}, \theta \right) - \left(\frac{\kappa}{\mathcal{D}_c} \rho_h^{n+\frac{1}{2}} \frac{3\mathbf{p}_h^n - \mathbf{p}_h^{n-1}}{2}, \theta \right) \\ &\quad - \mathcal{D} \left(\frac{e_c^{n+1} + e_c^n}{2}, \theta \right) + (\zeta_4^{n+\frac{1}{2}}, \theta), \end{aligned} \tag{4.12d}$$

$$\begin{aligned} \left(\frac{\mathbf{e}_p^{n+1} - \mathbf{e}_p^n}{\tau}, \beta \right) &= -\mathcal{L} \left(\frac{e_w^{n+1} + e_w^n}{2}, \beta \right) - \left(\Gamma \frac{\mathbf{e}_p^{n+1} + \mathbf{e}_p^n}{2}, \beta \right) - \Gamma_2 \left(\left| \frac{3\mathbf{p}^n - \mathbf{p}^{n-1}}{2} \right|^2 \mathbf{p}^{n+\frac{1}{2}} \right. \\ &\quad \left. - \left| \frac{3\mathbf{p}_h^n - \mathbf{p}_h^{n-1}}{2} \right|^2 \mathbf{p}_h^{n+\frac{1}{2}}, \beta \right) - SD \left(\frac{e_c^{n+1} + e_c^n}{2}, \beta \right) + (\zeta_5^{n+\frac{1}{2}}, \beta), \end{aligned} \tag{4.12e}$$

$$\left(\frac{1}{\mathcal{D}_p} \frac{e_w^{n+1} + e_w^n}{2}, r \right) = -\mathcal{K}(\mathbf{e}_p^{n+\frac{1}{2}}, r). \tag{4.12f}$$

Step 1. We take $v = \frac{\zeta_\rho^{n+1} + \zeta_\rho^n}{2}$ in (4.12a) and $\alpha = \frac{\zeta_q^{n+1} + \zeta_q^n}{2}$ in (4.12b), and sum up these two equations by the aid of Lemma 3.1 as well as (4.1) to get

$$\left(\frac{\zeta_\rho^{n+1} - \zeta_\rho^n}{\tau}, \frac{\zeta_\rho^{n+1} + \zeta_\rho^n}{2} \right) + \left(\frac{\zeta_q^{n+1} + \zeta_q^n}{2}, \frac{\zeta_q^{n+1} + \zeta_q^n}{2} \right) = \sum_{i=1}^5 R_i, \tag{4.13}$$

where

$$R_1 = \left(\frac{\eta_\rho^{n+1} - \eta_\rho^n}{\tau}, \frac{\zeta_\rho^{n+1} + \zeta_\rho^n}{2} \right) + \left(\frac{\eta_q^{n+1} + \eta_q^n}{2}, \frac{\zeta_q^{n+1} + \zeta_q^n}{2} \right),$$

$$\begin{aligned}
R_2 &= \left(\rho^{n+\frac{1}{2}} \frac{3\mathbf{p}^n - \mathbf{p}^{n-1}}{2} - \rho_h^{n+\frac{1}{2}} \frac{3\mathbf{p}_h^n - \mathbf{p}_h^{n-1}}{2}, \frac{\xi_q^{n+1} + \xi_q^n}{2} \right) \\
&= \left(\rho^{n+\frac{1}{2}} \frac{3\mathbf{e}_p^n - \mathbf{e}_p^{n-1}}{2}, \frac{\xi_q^{n+1} + \xi_q^n}{2} \right) + \left((\rho^{n+\frac{1}{2}} - \rho_h^{n+\frac{1}{2}}) \frac{3\mathbf{p}_h^n - \mathbf{p}_h^{n-1}}{2}, \frac{\xi_q^{n+1} + \xi_q^n}{2} \right), \\
R_3 &= g \left(\rho^{n+\frac{1}{2}} \left(1 - \frac{3\rho^n - \rho^{n-1}}{2} \right), \frac{\xi_\rho^{n+1} + \xi_\rho^n}{2} \right) - g \left(\rho_h^{n+\frac{1}{2}} \left(1 - \frac{3\rho_h^n - \rho_h^{n-1}}{2} \right), \frac{\xi_\rho^{n+1} + \xi_\rho^n}{2} \right) \\
&= g \left(\frac{e_\rho^{n+1} + e_\rho^n}{2}, \frac{\xi_\rho^{n+1} + \xi_\rho^n}{2} \right) - g \left(\rho^{n+\frac{1}{2}} \frac{3e_\rho^n - e_\rho^{n-1}}{2}, \frac{\xi_\rho^{n+1} + \xi_\rho^n}{2} \right) \\
&\quad - g \left(\frac{e_\rho^{n+1} + e_\rho^n}{2} \frac{3\rho_h^n - \rho_h^{n-1}}{2}, \frac{\xi_\rho^{n+1} + \xi_\rho^n}{2} \right), \\
R_4 &= -\mathcal{D} \left(\frac{\eta_\rho^{n+1} + \eta_\rho^n}{2}, \frac{\xi_q^{n+1} + \xi_q^n}{2} \right), \\
R_5 &= \left(\zeta_1^{n+\frac{1}{2}}, \frac{\xi_\rho^{n+1} + \xi_\rho^n}{2} \right) + \left(\zeta_2^{n+\frac{1}{2}}, \frac{\xi_q^{n+1} + \xi_q^n}{2} \right).
\end{aligned}$$

R_1 can be derived by the Schwarz inequality and Lemma 4.1,

$$R_1 \leq Ch^{k+1} \left(\|\xi_\rho^n\| + \|\xi_\rho^{n+1}\| + \left\| \frac{\xi_q^{n+1} + \xi_q^n}{2} \right\| \right).$$

Using hypothesis 3, Lemma 4.1 and (4.5), we obtain

$$R_2 \leq C(h^{k+1} + \|\xi_\rho^{n+1}\| + \|\xi_\rho^n\| + \|\xi_\rho^{n-1}\|) \left\| \frac{\xi_q^{n+1} + \xi_q^n}{2} \right\|,$$

where C depends on $\|\mathbf{p}_h^n\|_\infty, \|\mathbf{p}_h^{n-1}\|_\infty$. Similarly, using hypothesis 3, Lemma 4.1 and (4.5), we obtain

$$R_3 \leq C(h^{k+1} + \|\xi_\rho^{n+1}\| + \|\xi_\rho^n\| + \|\xi_\rho^{n-1}\|) (\|\xi_\rho^{n+1}\| + \|\xi_\rho^n\|),$$

where C depends on $\|\rho_h^n\|_\infty, \|\rho_h^{n-1}\|_\infty$. By Lemma 2.4, we have

$$R_4 \leq Ch^{k+1} \|\rho^{n+1}\|_{k+2} \left\| \frac{\xi_q^{n+1} + \xi_q^n}{2} \right\| + Ch^{k+1} \|\rho^n\|_{k+2} \left\| \frac{\xi_q^{n+1} + \xi_q^n}{2} \right\|.$$

Finally, for R_5 , we apply the Schwarz inequality to get

$$R_5 \leq C\tau^2 \left(\|\xi_\rho^{n+1}\| + \|\xi_\rho^n\| + \left\| \frac{\xi_q^{n+1} + \xi_q^n}{2} \right\| \right).$$

Substituting the above equations into (4.13) and with the help of Young's inequality, we

have

$$\begin{aligned}
 & \frac{1}{2} \|\zeta_\rho^{n+1}\|^2 - \frac{1}{2} \|\zeta_\rho^n\|^2 + \tau \left\| \frac{\zeta_q^{n+1} + \zeta_q^n}{2} \right\|^2 \\
 & \leq C\tau(h^{k+1} + \tau^2 + \|\zeta_\rho^{n+1}\| + \|\zeta_\rho^n\| + \|\zeta_\rho^{n-1}\|)(\|\zeta_\rho^{n+1}\| + \|\zeta_\rho^n\|) \\
 & \quad + C\tau(h^{k+1} + \tau^2 + \|\zeta_\rho^{n+1}\| + \|\zeta_\rho^n\| + \|\zeta_p^n\| + \|\zeta_p^{n-1}\|) \left\| \frac{\zeta_q^{n+1} + \zeta_q^n}{2} \right\| \\
 & \leq C\tau(\|\zeta_\rho^{n+1}\|^2 + \|\zeta_\rho^n\|^2 + \|\zeta_\rho^{n-1}\|^2 + \|\zeta_p^n\|^2 + \|\zeta_p^{n-1}\|^2) \\
 & \quad + \epsilon\tau \left\| \frac{\zeta_q^{n+1} + \zeta_q^n}{2} \right\|^2 + C\tau(h^{2k+2} + \tau^4).
 \end{aligned} \tag{4.14}$$

Step 2. We choose $\zeta = \frac{\zeta_c^{n+1} + \zeta_c^n}{2}$ in (4.12c) and $\theta = \frac{\zeta_u^{n+1} + \zeta_u^n}{2}$ in (4.12d), then sum up them by the aid of Lemma 3.1 as well as (4.1) to get

$$\begin{aligned}
 & \left(\frac{\zeta_c^{n+1} - \zeta_c^n}{\tau}, \frac{\zeta_c^{n+1} + \zeta_c^n}{2} \right) + \left(\frac{1}{\mathcal{D}_c} \frac{\zeta_u^{n+1} + \zeta_u^n}{2}, \frac{\zeta_u^{n+1} + \zeta_u^n}{2} \right) \\
 & \quad + \left(\frac{\zeta_c^{n+1} + \zeta_c^n}{2}, \frac{\zeta_c^{n+1} + \zeta_c^n}{2} \right) = \sum_{i=1}^5 \tilde{R}_i,
 \end{aligned} \tag{4.15}$$

where

$$\begin{aligned}
 \tilde{R}_1 &= \left(\frac{\eta_c^{n+1} - \eta_c^n}{\tau}, \frac{\zeta_c^{n+1} + \zeta_c^n}{2} \right) + \left(\frac{1}{\mathcal{D}_c} \frac{\eta_u^{n+1} + \eta_u^n}{2}, \frac{\zeta_u^{n+1} + \zeta_u^n}{2} \right), \\
 \tilde{R}_2 &= \left(\frac{e_\rho^{n+1} + e_\rho^n}{2}, \frac{\zeta_c^{n+1} + \zeta_c^n}{2} \right) + \left(\frac{\eta_c^{n+1} + \eta_c^n}{2}, \frac{\zeta_c^{n+1} + \zeta_c^n}{2} \right), \\
 \tilde{R}_3 &= \frac{\kappa}{\mathcal{D}_c} \left(\rho^{n+\frac{1}{2}} \frac{3\mathbf{p}^n - \mathbf{p}^{n-1}}{2} - \rho_h^{n+\frac{1}{2}} \frac{3\mathbf{p}_h^n - \mathbf{p}_h^{n-1}}{2}, \frac{\zeta_u^{n+1} + \zeta_u^n}{2} \right) \\
 &= \frac{\kappa}{\mathcal{D}_c} \left(\rho^{n+\frac{1}{2}} \frac{3\mathbf{e}_p^n - \mathbf{e}_p^{n-1}}{2}, \frac{\zeta_u^{n+1} + \zeta_u^n}{2} \right) + \frac{\kappa}{\mathcal{D}_c} \left((\rho^{n+\frac{1}{2}} - \rho_h^{n+\frac{1}{2}}) \frac{3\mathbf{p}_h^n - \mathbf{p}_h^{n-1}}{2}, \frac{\zeta_u^{n+1} + \zeta_u^n}{2} \right), \\
 \tilde{R}_4 &= \mathcal{D} \left(\frac{\eta_c^{n+1} + \eta_c^n}{2}, \frac{\zeta_u^{n+1} + \zeta_u^n}{2} \right), \\
 \tilde{R}_5 &= \left(\zeta_3^{n+\frac{1}{2}}, \frac{\zeta_c^{n+1} + \zeta_c^n}{2} \right) + \left(\zeta_4^{n+\frac{1}{2}}, \frac{\zeta_u^{n+1} + \zeta_u^n}{2} \right).
 \end{aligned}$$

By the Schwarz inequality and Lemma 4.1, we have

$$\tilde{R}_1 \leq Ch^{k+1} \left(\|\zeta_c^n\| + \|\zeta_c^{n+1}\| + \left\| \frac{\zeta_u^{n+1} + \zeta_u^n}{2} \right\| \right).$$

Following from Lemma 4.1, we can get

$$\tilde{R}_2 \leq C(h^{k+1} + \|\zeta_\rho^{n+1}\| + \|\zeta_\rho^n\|)(\|\zeta_c^{n+1}\| + \|\zeta_c^n\|).$$

Using hypothesis 2, hypothesis 3, Lemma 4.1 and (4.5), we obtain

$$\tilde{R}_3 \leq C(h^{k+1} + \|\zeta_\rho^{n+1}\| + \|\zeta_\rho^n\| + \|\zeta_p^n\| + \|\zeta_p^{n-1}\|) \left\| \frac{\zeta_u^{n+1} + \zeta_u^n}{2} \right\|,$$

where C depends on $\|\mathbf{p}_h^n\|_\infty, \|\mathbf{p}_h^{n-1}\|_\infty$. By Lemma 2.4, we have

$$\tilde{R}_4 \leq Ch^{k+1} \|c^{n+1}\|_{k+2} \left\| \frac{\zeta_u^{n+1} + \zeta_u^n}{2} \right\| + Ch^{k+1} \|c^n\|_{k+2} \left\| \frac{\zeta_u^{n+1} + \zeta_u^n}{2} \right\|.$$

Finally, for \tilde{R}_5 , we apply the Schwarz inequality to get

$$\tilde{R}_5 \leq C\tau^2 \left(\|\zeta_c^{n+1}\| + \|\zeta_c^n\| + \left\| \frac{\zeta_u^{n+1} + \zeta_u^n}{2} \right\| \right).$$

Substituting the above equations into (4.15) and with the help of Young's inequality, we have

$$\begin{aligned} & \frac{1}{2} \|\zeta_c^{n+1}\|^2 - \frac{1}{2} \|\zeta_c^n\|^2 + \tau \left\| \frac{1}{\sqrt{\mathcal{D}_c}} \frac{\zeta_u^{n+1} + \zeta_u^n}{2} \right\|^2 \\ & \leq C\tau(h^{k+1} + \tau^2 + \|\zeta_\rho^{n+1}\| + \|\zeta_\rho^n\|) (\|\zeta_c^{n+1}\| + \|\zeta_c^n\|) \\ & \quad + C\tau(h^{k+1} + \tau^2 + \|\zeta_\rho^{n+1}\| + \|\zeta_\rho^n\| + \|\zeta_p^n\| + \|\zeta_p^{n-1}\|) \left\| \frac{\zeta_u^{n+1} + \zeta_u^n}{2} \right\| \\ & \leq C\tau (\|\zeta_\rho^{n+1}\|^2 + \|\zeta_\rho^n\|^2 + \|\zeta_c^{n+1}\|^2 + \|\zeta_c^n\|^2 + \|\zeta_p^n\|^2 + \|\zeta_p^{n-1}\|^2) \\ & \quad + \epsilon\tau \left\| \frac{1}{\sqrt{\mathcal{D}_c}} \frac{\zeta_u^{n+1} + \zeta_u^n}{2} \right\|^2 + C\tau(h^{2k+2} + \tau^4). \end{aligned} \tag{4.16}$$

Step 3. Choosing $\beta = \frac{\zeta_p^{n+1} + \zeta_p^n}{2}$ in (4.12e) and $r = \frac{\zeta_w^{n+1} + \zeta_w^n}{2}$ in (4.12f), and then summing these two equations by the aid of Lemma 3.1 as well as (4.1), we get

$$\begin{aligned} & \left(\frac{\zeta_p^{n+1} - \zeta_p^n}{\tau}, \frac{\zeta_p^{n+1} + \zeta_p^n}{2} \right) + \frac{1}{\mathcal{D}_p} \left(\frac{\zeta_w^{n+1} + \zeta_w^n}{2}, \frac{\zeta_w^{n+1} + \zeta_w^n}{2} \right) + \Gamma \left(\frac{\zeta_p^{n+1} + \zeta_p^n}{2}, \frac{\zeta_p^{n+1} + \zeta_p^n}{2} \right) \\ & + \Gamma_2 \left(\left| \frac{3\mathbf{p}_h^n - \mathbf{p}_h^{n-1}}{2} \right|^2 \frac{\zeta_p^{n+1} + \zeta_p^n}{2}, \frac{\zeta_p^{n+1} + \zeta_p^n}{2} \right) = \sum_{i=1}^6 T_i, \end{aligned} \tag{4.17}$$

where

$$\begin{aligned} T_1 &= \left(\frac{\eta_p^{n+1} - \eta_p^n}{\tau}, \frac{\zeta_p^{n+1} + \zeta_p^n}{2} \right) + \frac{1}{\mathcal{D}_p} \left(\frac{\eta_w^{n+1} + \eta_w^n}{2}, \frac{\zeta_w^{n+1} + \zeta_w^n}{2} \right), \\ T_2 &= \Gamma \left(\frac{\eta_p^{n+1} + \eta_p^n}{2}, \frac{\zeta_p^{n+1} + \zeta_p^n}{2} \right), \end{aligned}$$

$$\begin{aligned}
 T_3 &= -\Gamma_2 \left(\left(\left| \frac{3\mathbf{p}^n - \mathbf{p}^{n-1}}{2} \right| + \left| \frac{3\mathbf{p}_h^n - \mathbf{p}_h^{n-1}}{2} \right| \right) \left(\left| \frac{3\mathbf{p}^n - \mathbf{p}^{n-1}}{2} \right| - \left| \frac{3\mathbf{p}_h^n - \mathbf{p}_h^{n-1}}{2} \right| \right) \frac{\mathbf{p}^{n+1} + \mathbf{p}^n}{2}, \right. \\
 &\quad \left. \frac{\bar{\zeta}_p^{n+1} + \bar{\zeta}_p^n}{2} \right) + \Gamma_2 \left(\left| \frac{3\mathbf{p}_h^n - \mathbf{p}_h^{n-1}}{2} \right|^2 \frac{\eta_p^{n+1} + \eta_p^n}{2}, \frac{\bar{\zeta}_p^{n+1} + \bar{\zeta}_p^n}{2} \right), \\
 T_4 &= -SD \left(\frac{e_c^{n+1} + e_c^n}{2}, \frac{\bar{\zeta}_p^{n+1} + \bar{\zeta}_p^n}{2} \right), \\
 T_5 &= \mathcal{K} \left(\frac{\eta_p^{n+1} + \eta_p^n}{2}, \frac{\bar{\zeta}_w^{n+1} + \bar{\zeta}_w^n}{2} \right), \\
 T_6 &= \left(\zeta_5^{n+\frac{1}{2}}, \frac{\bar{\zeta}_p^{n+1} + \bar{\zeta}_p^n}{2} \right).
 \end{aligned}$$

We can obtain the estimate of T_1 by Lemma 4.1 and the Schwarz inequality,

$$T_1 \leq Ch^{k+1} \left(\|\bar{\zeta}_p^{n+1}\| + \|\bar{\zeta}_p^n\| + \left\| \frac{\bar{\zeta}_w^{n+1} + \bar{\zeta}_w^n}{2} \right\| \right).$$

We can estimate T_2 by Lemma 4.1,

$$T_2 \leq Ch^{k+1} (\|\bar{\zeta}_p^{n+1}\| + \|\bar{\zeta}_p^n\|).$$

Following from hypothesis 2, hypothesis 3, Lemma 4.1 and (4.5), then we can obtain

$$T_3 \leq C(h^{k+1} + \|\bar{\zeta}_p^n\| + \|\bar{\zeta}_p^{n-1}\|) (\|\bar{\zeta}_p^{n+1}\| + \|\bar{\zeta}_p^n\|).$$

Here, we use

$$\begin{aligned}
 \left\| \left| \frac{3\mathbf{p}^n - \mathbf{p}^{n-1}}{2} \right| - \left| \frac{3\mathbf{p}_h^n - \mathbf{p}_h^{n-1}}{2} \right| \right\| &\leq \left\| \frac{3\mathbf{p}^n - \mathbf{p}^{n-1}}{2} - \frac{3\mathbf{p}_h^n - \mathbf{p}_h^{n-1}}{2} \right\| \\
 &= \left\| \frac{3\mathbf{p}^n - \mathbf{p}^{n-1}}{2} - \frac{3\mathbf{p}_h^n - \mathbf{p}_h^{n-1}}{2} \right\|
 \end{aligned}$$

and C depends on $\|\mathbf{p}_h^n\|_\infty, \|\mathbf{p}_h^{n-1}\|_\infty$. Refer to Lemma 4.2 and Lemma 2.1, we have

$$T_4 \leq C(h^{k+1} + \|\bar{\zeta}_c^{n+1}\| + \|\bar{\zeta}_c^n\|) \left(h^{k+1} + \left\| \frac{\bar{\zeta}_w^{n+1} + \bar{\zeta}_w^n}{2} \right\| \right).$$

Using the Lemma 2.4, we get

$$T_5 \leq Ch^{k+1} \|\mathbf{p}^{n+1}\|_{k+2} \left\| \frac{\bar{\zeta}_w^{n+1} + \bar{\zeta}_w^n}{2} \right\| + Ch^{k+1} \|\mathbf{p}^n\|_{k+2} \left\| \frac{\bar{\zeta}_w^{n+1} + \bar{\zeta}_w^n}{2} \right\|.$$

The estimate of T_6 follows from the Schwarz inequality that

$$T_6 \leq C\tau^2 (\|\bar{\zeta}_p^{n+1}\| + \|\bar{\zeta}_p^n\|).$$

Substituting the above equations into (4.17) and with the help of Young's inequality, we have

$$\begin{aligned}
& \frac{1}{2} \|\xi_p^{n+1}\|^2 - \frac{1}{2} \|\xi_p^n\|^2 + \tau \left\| \frac{1}{\sqrt{\mathcal{D}_p}} \frac{\xi_w^{n+1} + \xi_w^n}{2} \right\|^2 \\
& \leq C\tau(h^{k+1} + \tau^2 + \|\xi_p^n\| + \|\xi_p^{n-1}\|)(\|\xi_p^{n+1}\| + \|\xi_p^n\|) \\
& \quad + C\tau(h^{k+1} + \|\xi_c^{n+1}\| + \|\xi_c^n\|) \left\| \frac{\xi_w^{n+1} + \xi_w^n}{2} \right\| \\
& \leq C\tau(\|\xi_c^{n+1}\|^2 + \|\xi_c^n\|^2 + \|\xi_p^{n+1}\|^2 + \|\xi_p^n\|^2 + \|\xi_p^{n-1}\|^2) \\
& \quad + \epsilon\tau \left\| \frac{1}{\sqrt{\mathcal{D}_p}} \frac{\xi_w^{n+1} + \xi_w^n}{2} \right\|^2 + C\tau(h^{2k+2} + \tau^4). \tag{4.18}
\end{aligned}$$

Taking $\epsilon = \frac{1}{8}$ and combining (4.14), (4.16), (4.18), then summing them over n , we obtain

$$\begin{aligned}
& \frac{1}{2} \|\xi_\rho^{n+1}\|^2 + \frac{1}{2} \|\xi_c^{n+1}\|^2 + \frac{1}{2} \|\xi_p^{n+1}\|^2 + \frac{7\tau}{8} \sum_{m=1}^n \left\| \frac{\xi_q^{m+1} + \xi_q^m}{2} \right\|^2 \\
& \quad + \frac{7\tau}{8} \sum_{m=1}^n \left\| \frac{1}{\sqrt{\mathcal{D}_c}} \frac{\xi_u^{m+1} + \xi_u^m}{2} \right\|^2 + \frac{7\tau}{8} \sum_{m=1}^n \left\| \frac{1}{\sqrt{\mathcal{D}_p}} \frac{\xi_w^{m+1} + \xi_w^m}{2} \right\|^2 \\
& \leq C\tau \sum_{m=1}^n (\|\xi_\rho^{m+1}\|^2 + \|\xi_\rho^m\|^2 + \|\xi_\rho^{m-1}\|^2 + \|\xi_c^m\|^2 + \|\xi_c^{m+1}\|^2 + \|\xi_p^{m+1}\|^2 \\
& \quad + \|\xi_p^m\|^2 + \|\xi_p^{m-1}\|^2) + C(h^{2k+2} + \tau^4) + Q_1, \tag{4.19}
\end{aligned}$$

where

$$Q_1 = \frac{1}{2} \|\xi_\rho^1\|^2 + \frac{1}{2} \|\xi_c^1\|^2 + \frac{1}{2} \|\xi_p^1\|^2. \tag{4.20}$$

When proving the theorem 4.1, we assume $n=0$ to obtain

$$\begin{aligned}
& \frac{1}{2} \|\xi_\rho^1\|^2 + \frac{1}{2} \|\xi_c^1\|^2 + \frac{1}{2} \|\xi_p^1\|^2 + \tau \|\xi_q^1\|^2 + \tau \left\| \frac{1}{\sqrt{\mathcal{D}_c}} \xi_u^1 \right\|^2 + \tau \left\| \frac{1}{\sqrt{\mathcal{D}_p}} \xi_w^1 \right\|^2 \\
& \leq C\tau(h^{k+1} + \tau + \|\xi_\rho^1\|) \|\xi_\rho^1\| + C\tau(h^{k+1} + \tau + \|\xi_\rho^1\|) \|\xi_q^1\| + C\tau(h^{k+1} + \tau + \|\xi_\rho^1\|) \|\xi_c^1\| \\
& \quad + C\tau(h^{k+1} + \tau + \|\xi_\rho^1\|) \|\xi_u^1\| + C\tau(h^{k+1} + \tau) \|\xi_p^1\| + C\tau(h^{k+1} + \|\xi_c^1\|) \|\xi_w^1\| \\
& \leq \epsilon(\|\xi_\rho^1\|^2 + \|\xi_c^1\|^2 + \|\xi_p^1\|^2) + \epsilon\tau \|\xi_q^1\|^2 + \epsilon\tau \left\| \frac{1}{\sqrt{\mathcal{D}_c}} \xi_u^1 \right\|^2 + \epsilon\tau \left\| \frac{1}{\sqrt{\mathcal{D}_p}} \xi_w^1 \right\|^2 + C\tau h^{2k+2} + C\tau^4,
\end{aligned}$$

where τ and ϵ is small enough. Then we get

$$\|\xi_\rho^1\|^2 + \|\xi_c^1\|^2 + \|\xi_p^1\|^2 + \tau \|\xi_q^1\|^2 + \tau \|\xi_u^1\|^2 + \tau \|\xi_w^1\|^2 \leq C(h^{2k+2} + \tau^4).$$

Therefore,

$$Q_1 \leq C(h^{2k+2} + \tau^4).$$

Applying the discrete Gronwall's inequality to (4.19) and under the condition $C\tau \leq \frac{1}{4}$, we can obtain

$$\begin{aligned} & \|\tilde{\zeta}_\rho^n\|^2 + \|\tilde{\zeta}_c^n\|^2 + \|\tilde{\zeta}_p^n\|^2 + \tau \sum_{m=2}^n \left\| \frac{\tilde{\zeta}_q^m + \tilde{\zeta}_q^{m-1}}{2} \right\|^2 + \tau \sum_{m=2}^n \left\| \frac{\tilde{\zeta}_u^m + \tilde{\zeta}_u^{m-1}}{2} \right\|^2 \\ & + \tau \sum_{m=2}^n \left\| \frac{\tilde{\zeta}_w^m + \tilde{\zeta}_w^{m-1}}{2} \right\|^2 \leq C(h^{2k+2} + \tau^4), \end{aligned} \tag{4.21}$$

which further yields the following error equation

$$\begin{aligned} & \|e_\rho^n\|^2 + \|e_c^n\|^2 + \|e_p^n\|^2 + \tau \sum_{m=2}^n \left\| \frac{e_q^m + e_q^{m-1}}{2} \right\|^2 + \tau \sum_{m=2}^n \left\| \frac{e_u^m + e_u^{m-1}}{2} \right\|^2 \\ & + \tau \sum_{m=2}^n \left\| \frac{e_w^m + e_w^{m-1}}{2} \right\|^2 \leq C(h^{2k+2} + \tau^4). \end{aligned} \tag{4.22}$$

In the theoretical analysis, the proof of the a priori assumption is necessary. Since $\|\tilde{\zeta}_p^0\| = 0$ and $\|\tilde{\zeta}_\rho^0\| = 0$, by $k \geq 1$ and a use of Lemma 4.1, we have

$$\|e_p^0\| + \|e_\rho^0\| = \|\eta_p^0\| + \|\eta_\rho^0\| \leq Ch^{k+1} \leq h^{1+\delta},$$

if h is sufficiently small. Assuming that (4.4) holds for arbitrary given n , it follows that theorem 4.2 holds for the bounding constant that is independent of n and h .

$$\|e_p^{n+1}\| + \|e_\rho^{n+1}\| \leq C(h^{k+1} + \tau^2) \leq h^{1+\delta}. \tag{4.23}$$

Therefore, the a priori assumption is plausible.

5 Numerical experiments

In this section, several numerical examples are provided to illustrate the accuracy and capability of the IMEX-LDG schemes (3.4a)-(3.6b) and (3.8a)-(3.10b) for the growth-mediated autochemotactic pattern formation model. The interplay of growth rate and chemotactic drift of the cells with respect to the self-secreted signaling chemicals is studied in the examples. Example 5.2 was performed in [10] by a first-order semi-implicit time discretization, and when $g = 0$ in the density equation (1.1a), a mass-preserving characteristic finite element method was considered therein. A finite difference method and a first-order accurate Euler time method are used to simulate Examples 5.3, 5.4, 5.6 in [11, 13]. In this paper, we use fully-discrete IMEX-LDG(1,2) numerical method in the simulations, which is a second-order accurate numerical method. The IMEX time integration method constructed in this paper is decoupled and linear, which saves a lot of computational costs in long time simulations.

5.1 Accuracy verification

Example 5.1 (Accuracy verification of the IMEX-LDG discretizations.). We first study the accuracy of the fully-discrete IMEX-LDG method for the growth-mediated autochemotactic pattern formation model (1.1a)-(1.1c). The parameters are chosen as $\kappa = 1$, $S = 0.1$, $\Gamma = 1$, $\Gamma_2 = 10$, $g = 1.0$. The results are presented for $\mathcal{D}_p = 2$, $\mathcal{D}_c = 1$ and $\mathcal{D}_p = 0.02$, $\mathcal{D}_c = 0.01$, respectively. We choose the exact smooth solution as

$$\rho(x, y, t) = e^{-t} \sin(x) \sin(y), \quad c(x, y, t) = e^{-t} \cos(x) \cos(y), \quad (5.1a)$$

$$\mathbf{p}(x, y, t) = e^{-t} [\sin(x) \cos(y), \cos(x) \sin(y)], \quad (x, y) \in [0, 2\pi]^2, \quad (5.1b)$$

to satisfy Eqs. (1.1a)-(1.1c) with source terms. The initial conditions are computed from (5.1). We impose periodic boundary conditions in this example.

The computational domain is partitioned by a uniform rectangular mesh of $N_x \times N_y$ cells. In this example, we take $N_x = N_y \triangleq N$ for simplicity. Fully-discrete IMEX-LDG(1,1) and IMEX-LDG(1,2) time-marching schemes are applied in this example. The time step is chosen as $\Delta t = 0.1h$, with h the mesh size. Table 1 shows the numerical results for the accuracy test with $\mathcal{D}_c = 1$, $\mathcal{D}_p = 2$ and Table 2 shows those of the convection-dominated case with $\mathcal{D}_c = 0.01$, $\mathcal{D}_p = 0.02$. The optimal order of accuracy is observed for IMEX-LDG(1,1) and IMEX-LDG(1,2) of the growth-mediated autochemotactic pattern formation model, respectively.

Table 1: Accuracy verification of the growth-mediated autochemotactic pattern formation model (1.1a)-(1.1c) in L^2 norm at terminal time $T = 0.2$. The parameters are chosen as $\kappa = 1$, $S = 0.1$, $\Gamma = 1$, $\Gamma_2 = 10$, $g = 1.0$.

	N	$\ \rho - \rho_h\ _2$	order	$\ c - c_h\ _2$	order	$\ \mathbf{p} - \mathbf{p}_h\ _2$	order
IMEX-LDG(1,1)	8	5.73E-01	–	1.20E-00	–	5.47E-01	–
	16	1.58E-01	1.85	3.17E-01	1.92	1.82E-01	1.58
	32	5.07E-02	1.64	8.79E-02	1.85	6.94E-02	1.39
	64	2.04E-02	1.31	2.88E-02	1.60	3.18E-02	1.12
IMEX-LDG(1,2)	8	5.68E-01	–	1.20E-00	–	5.99E-01	–
	16	1.42E-01	2.00	3.06E-01	1.96	1.39E-01	2.10
	32	3.55E-02	2.00	7.71E-02	1.99	3.53E-02	1.98
	64	8.87E-03	2.00	1.93E-02	1.99	8.96E-03	1.98

The rest several examples are provided to simulate the growth-mediated autochemotactic pattern formation in the chemotaxis case and chemorepulsion case. In Example 5.5, the parameters of Eqs. (1.1a)-(1.1c) are taken as

$$\mathcal{D}_c = 0.02, \quad \Gamma = 1.0, \quad \mathcal{D}_p = 0.01. \quad (5.2)$$

In the remaining examples, the parameters of Eqs. (1.1a)-(1.1c) are chosen as

$$\mathcal{D}_c = 1.0, \quad \Gamma = 1.0, \quad \mathcal{D}_p = 1.0. \quad (5.3)$$

Table 2: Accuracy verification of the growth-mediated autochemotactic pattern formation model in L^2 norm for the convection-dominated case at terminal time $T=0.2$. The parameters are chosen as $\kappa=1, S=0.1, \Gamma=1, \Gamma_2=10, g=1.0$.

	N	$\ \rho - \rho_h\ _2$	order	$\ c - c_h\ _2$	order	$\ \mathbf{p} - \mathbf{p}_h\ _2$	order
IMEX-LDG(1,1)	8	5.73E-01	-	1.15E-00	-	4.83E-01	-
	16	1.58E-01	1.85	3.66E-01	1.65	1.52E-01	1.67
	32	5.11E-02	1.64	1.15E-01	1.67	5.74E-02	1.40
	64	2.06E-02	1.31	3.22E-02	1.84	2.60E-02	1.13
	128	9.69E-03	1.09	1.20E-02	1.42	1.30E-02	1.00
IMEX-LDG(1,2)	8	5.67E-01	-	1.16E-00	-	5.56E-01	-
	16	1.42E-01	2.00	3.67E-01	1.66	1.20E-01	2.21
	32	3.55E-02	2.00	1.10E-01	1.74	3.10E-02	1.95
	64	8.87E-03	2.00	2.42E-02	2.19	8.33E-03	1.90
	128	2.21E-03	2.00	5.23E-03	2.21	2.17E-03	1.94

The initial conditions are chosen as

$$\rho(x,y,0) = 1 + 10^{-4}(2rand(0,1) - 1), \quad c(x,y,0) = 1 + 10^{-4}(2rand(0,1) - 1), \quad (5.4a)$$

$$p_1(x,y,0) = 10^{-2}(2rand(0,1) - 1), \quad p_2(x,y,0) = 10^{-2}(2rand(0,1) - 1), \quad (5.4b)$$

where $rand(0,1)$ represents the number sampled uniformly at random from $[0,1]$. The computational domain is $\Omega = [0,100]^2$. Periodic boundary conditions are applied to the examples.

5.2 Chemoattraction case

When $S > 0$, bacteria propel themselves toward the self-secreted chemicals and form aggregates. As feedback, when the bacteria aggregate, more chemicals are produced which thereby attract more bacteria. This process means chemoattraction.

Example 5.2 (Absence and presence of growth dynamics). The parameters in Eqs. (1.1a)-(1.1c) are chosen as $\Gamma_2=10, S=10, \kappa=1$. Simulations are presented for $g=0$ in the absence of any growth dynamics and $g=0.1$ in the presence of growth dynamics, respectively.

We plot the contours of density of the bacteria in Fig. 1 for $g=0$ and 0.1 , respectively. Figs. 1(a) and (b) show that when $g=0$, the bacterial droplets aggregate continuously with time. The formation of stationary spot patterns of well attained steady state sizes are observed in Figs. 1(c) and (d) when $g=0.1$. The mass with time evolution is displayed in Fig. 2. Fig. 2 indicates that the total mass is conserved for $g=0$, while decreases for $g=0.1$. These results are similar to those in [11, 13].

Example 5.3 (Low value of Γ_2). Next, we perform simulations by decreasing the value of Γ_2 , for example $\Gamma_2=0.1$. The parameters in Eqs. (1.1a)-(1.1c) are chosen as $S=10, \kappa=0$. The parameter g is chosen as $0.1, 1$, and 1.5 .

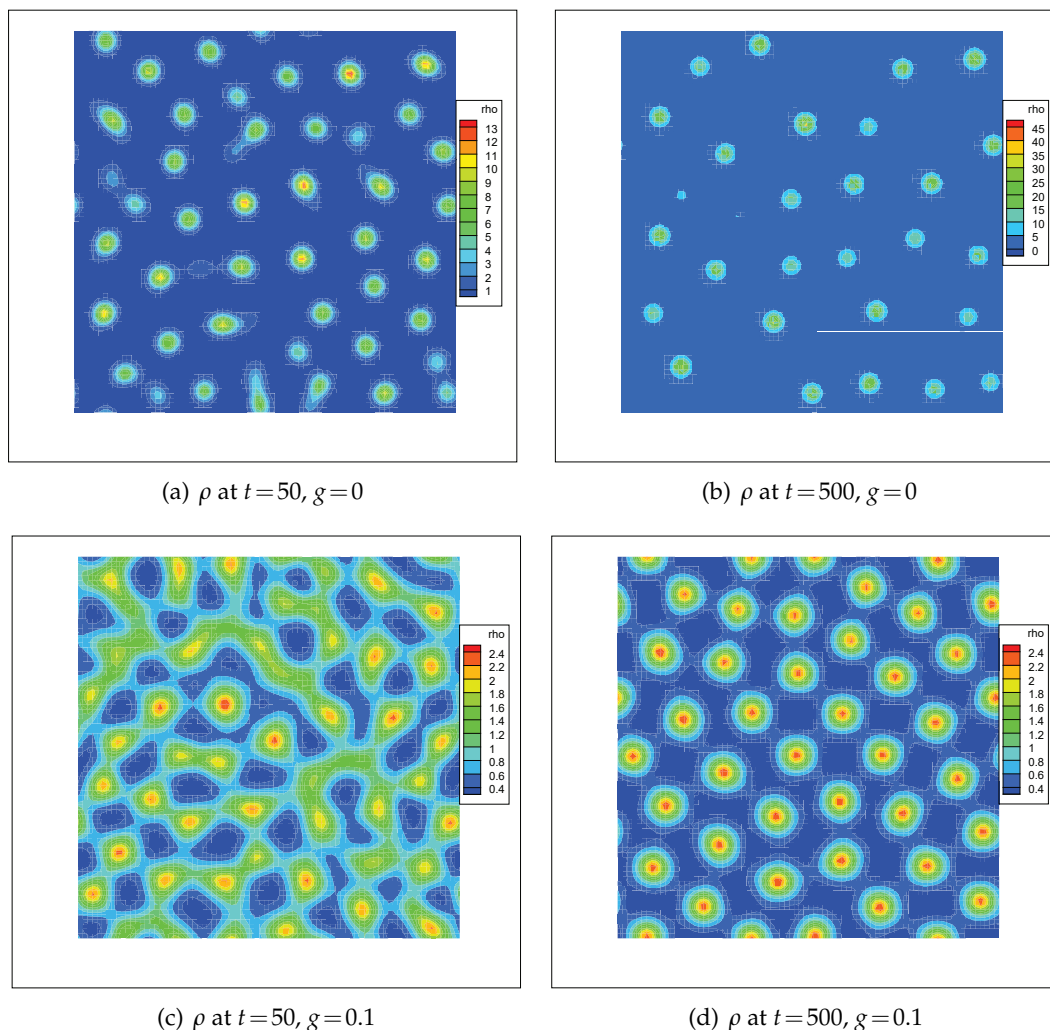


Figure 1: Density at different times in Example 5.2 for $g=0$ and $g=0.1$. The parameters are chosen as $\Gamma_2=10$, $S=10$, and $\kappa=1.0$. All other parameters are the same as in (5.3).

Fig. 3 shows that spots, stripes and inverted spots are obtained for $g=0.1, 1.0$ and 1.5 , respectively. The results again agree with those in [11, 13].

Example 5.4 (Concentric ring patterns). In this example, we study the pattern development in a growing colony by an initial inoculation of small bacterial droplets at the center of the domain. The initial conditions are given by

$$\rho(x,y,0) = e^{-20(x-50)^2-20(y-50)^2}, \quad c(x,y,0) = 1 + 10^{-4}(2\text{rand}(0,1) - 1), \quad (5.5a)$$

$$p_1(x,y,0) = 10^{-2}(2\text{rand}(0,1) - 1), \quad p_2(x,y,0) = 10^{-2}(2\text{rand}(0,1) - 1). \quad (5.5b)$$

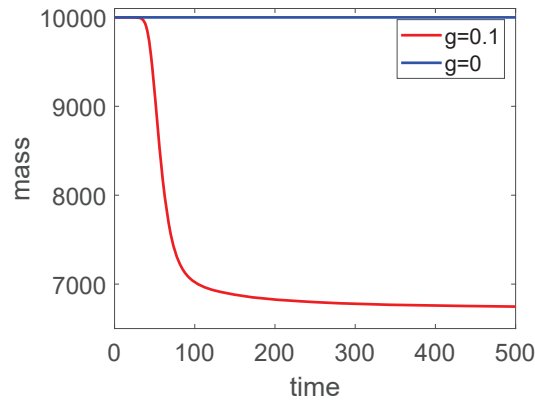


Figure 2: Time evolution of mass in Example 5.2. The parameters are chosen as $\Gamma_2=10$, $S=10$, $\kappa=1.0$. All other parameters are the same as in (5.3).

We take the parameters in Eqs. (1.1a)-(1.1c) as $\Gamma_2=10$, $\kappa=0.5$, $g=0.5$. The value of S is taken as $S=40$. All other parameters are kept the same as in (5.3). This example is motivated by the formation of concentric ring patterns observed in [1, 16] and the numerical verifications of [13].

The initial condition (5.5) means that a droplet of bacterial emerges at the center of the domain. Fig. 4 shows time evolution of the droplet of bacterial, and the colony develops concentric rings of bacterial density. Growth makes bacteria move away from the center of the domain, but chemoattraction holds them together. Similar to [13], we find destabilization of inner rings into small spot like structures.

Example 5.5 (The convection-dominated case). We do simulations for Example 5.2 with small values $\mathcal{D}_c=0.02$, $\mathcal{D}_p=0.01$. The rest of parameters are chosen the same as in Example 5.2. The stationary spot pattern with steady state sizes is displayed in Fig. 5 at final time. Fig. 6 shows that the total mass decreases for the autochemotactic pattern formation model with $g=0.1$.

5.3 Chemorepulsion case

When $S < 0$, bacteria flee away from the self-secreted signaling molecules. Such a process means chemorepulsion.

Example 5.6 (Growth dynamics). The parameters in Eqs. (1.1a)-(1.1c) are chosen as $\Gamma_2=10$, $\kappa=0.5$, $S=-15$.

We plot the contour of density of the active colloids at different times in Fig. 7 for $g=0.1$ and $g=4$, respectively. Fig. 7 shows that the small perturbation of the initial

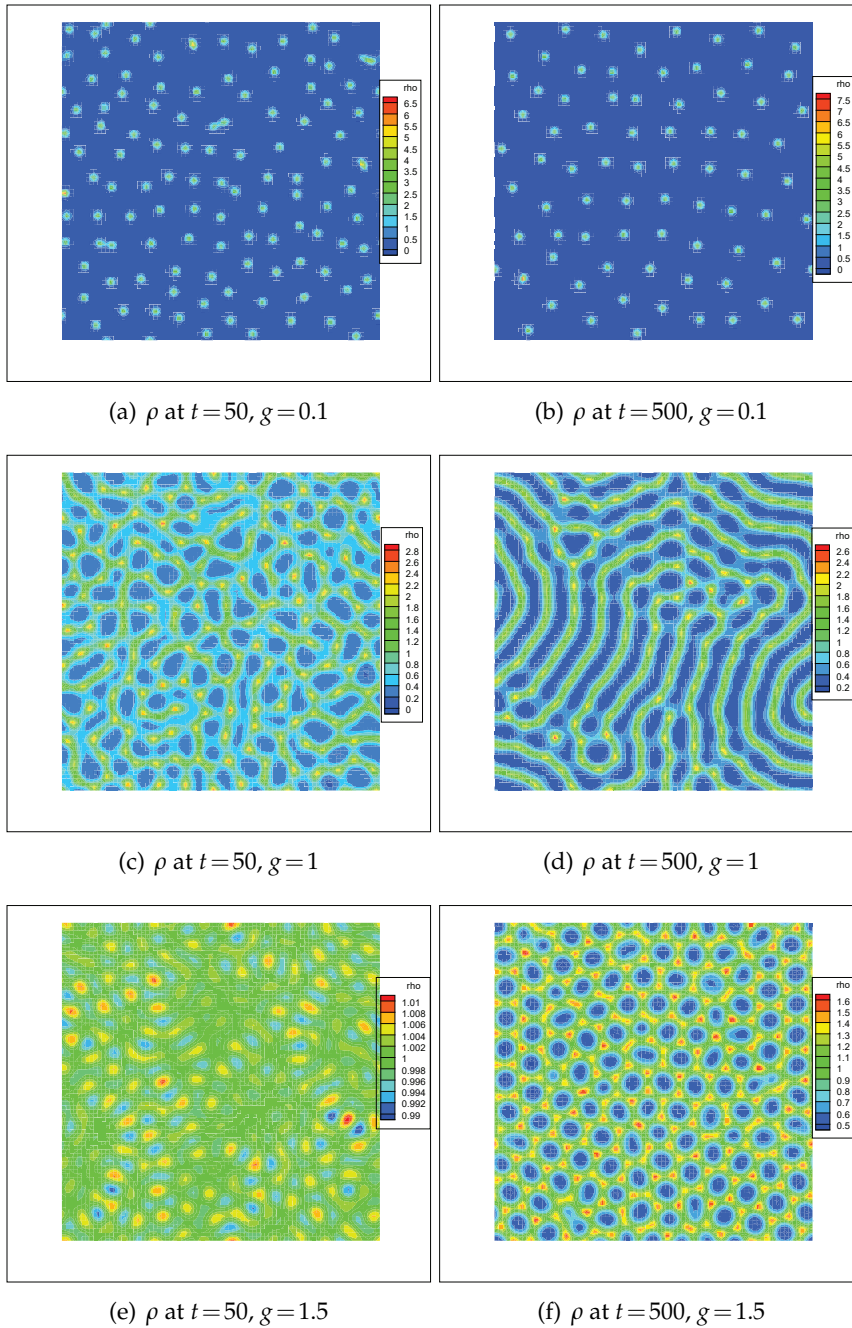


Figure 3: Density at different times in Example 5.3 for $g=0.1, 1.0$ and $g=1.5$. The parameters are $\Gamma_2=0.1, S=10, \kappa=0$. All other parameters are the same as in (5.3).

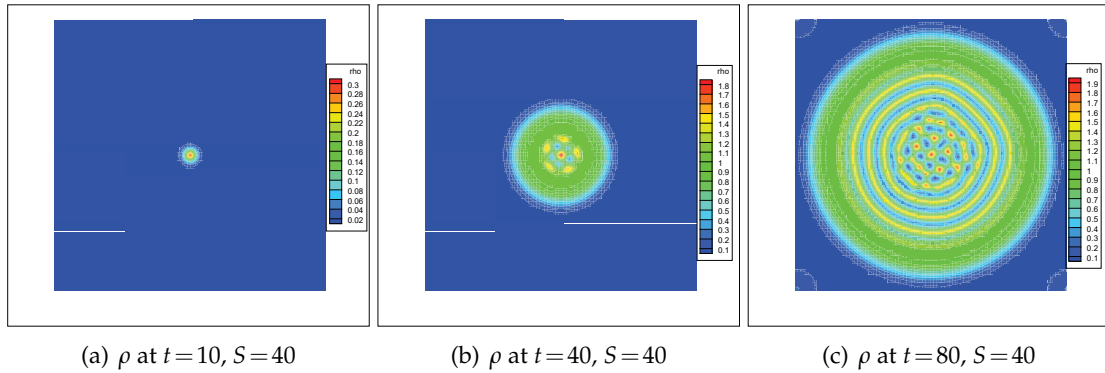


Figure 4: Density at different times in Example 5.4 for $S=40$. The parameters are chosen as $\Gamma_2=10, \kappa=0.5, g=0.5$. All other parameters are the same as in (5.3).

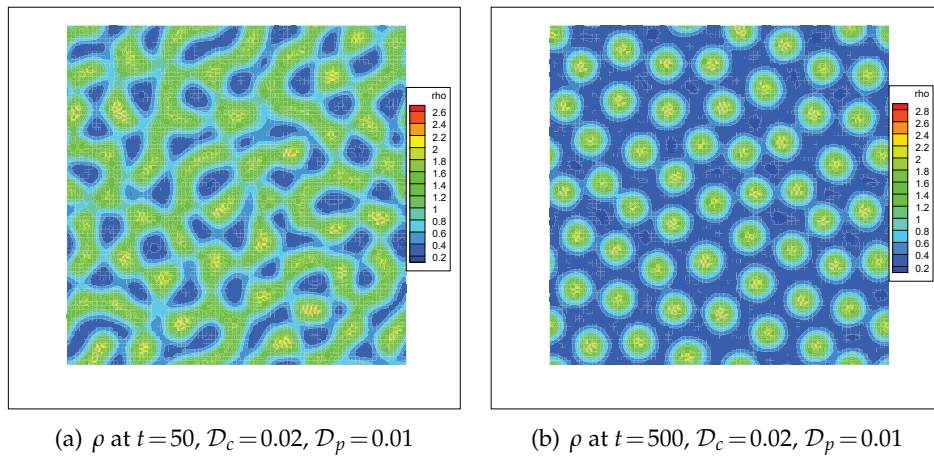


Figure 5: Density at different times in Example 5.5. The parameters are chosen as $\mathcal{D}_c=0.02, \mathcal{D}_p=0.01, \Gamma_2=10, S=10, \kappa=1.0, \Gamma=1.0$ and $g=0.1$.

uniform density develops clustering and pattern formation and finally a special order of the clustering and pattern shows up. The numerical mass is displayed in Fig. 8 during the simulations, which shows that the stable state can be obtained earlier for larger value of g . The results agree with those in [11, 13].

6 Concluding remarks

We have studied the IMEX-LDG methods for the growth-mediated autochemotactic pattern formation model. Two time integrations of both first-order and second-order accuracy are constructed, and error estimates of the IMEX-LDG schemes are derived. The

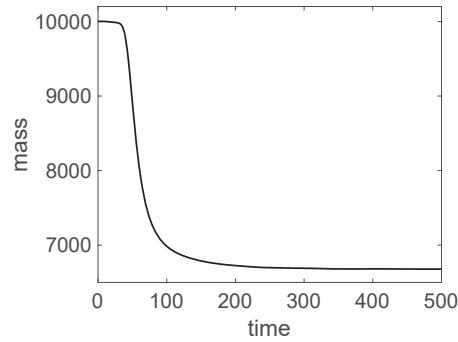


Figure 6: Time evolution of mass in Example 5.5. The parameters are chosen as $D_c=0.02$, $D_p=0.01$, $\Gamma_2=10$, $S=10$, $\kappa=1.0$, $\Gamma=1.0$ and $g=0.1$.

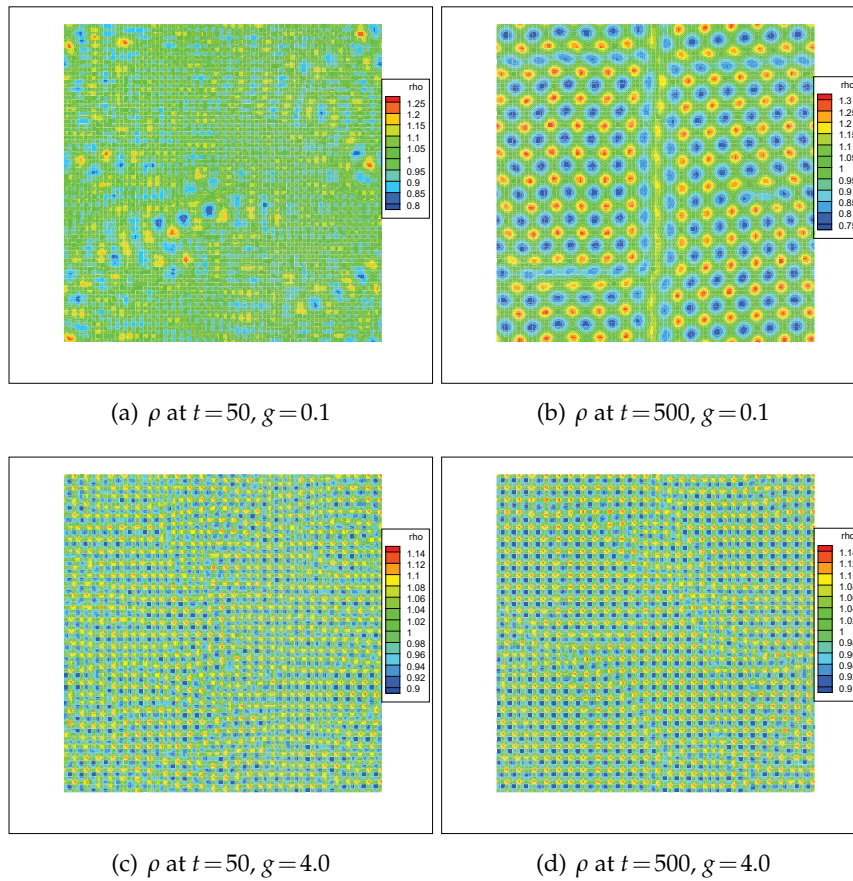


Figure 7: Density at different times in Example 5.6 for $g=0.1$ and $g=4.0$, respectively. The parameters are $\Gamma_2=10$, $\kappa=0.5$, $S=-15$. All other parameters are the same as in (5.3).

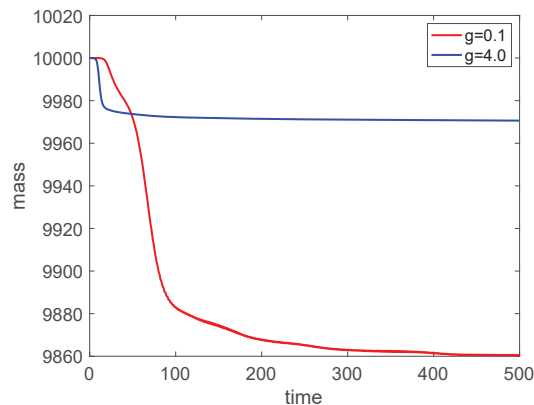


Figure 8: Time evolution of mass for different values of g in Example 5.6. The parameters are $\Gamma_2=10$, $\kappa=0.5$, $S=-15$. All other parameters are the same as in (5.3).

decoupled linear time integration methods constructed in this paper are computationally efficient. The theoretical analysis and capabilities for the simulations in applications are verified by ample numerical experiments. The numerical tests in Example 5.1 and 5.5 indicate that our IMEX-LDG methods are also suitable for the autochemotactic pattern formation model with low value of \mathcal{D}_c and \mathcal{D}_p . In our future work, the positivity-preserving technique of the density of the model will be explored.

Acknowledgements

This work is supported by National Natural Science Foundation of China (Grant No. 11801569), Natural Science Foundation of Shandong Province (CN) (Grant No. ZR2021MA001) and the Fundamental Research Funds for the Central Universities (Grant Nos. 22CX03025A and 22CX03020A).

References

- [1] M. P. BRENNER, L. S. LEVITOV AND E. O. BUDRENE, *Physical mechanisms for chemotactic pattern formation by bacteria*, *Biophys. J.*, 74 (1998), pp. 1677–1693.
- [2] E. O. BUDRENE AND H. C. BERG, *Generic modelling of cooperative growth patterns in bacterial colonies*, *Nature*, 349 (1991), p. 630.
- [3] F. BASSI AND S. REBAY, *A high-order accurate discontinuous finite element method for the numerical solution of the compressible Navier-Stokes equations*, *J. Comput. Phys.*, 131 (1997), pp. 267–279.
- [4] B. COCKBURN AND C.-W. SHU, *The local discontinuous Galerkin method for time-dependent convection-diffusion systems*, *SIAM J. Numer. Anal.*, 35 (1998), pp. 2440–2463.

- [5] P. CIARLET, *The Finite Element Method for Elliptic Problems*, Amsterdam-New York: North Holland, 1978.
- [6] P. CASTILLO, B. COCKBURN, I. PERUGIA AND D. SCHÖTZAU, *Superconvergence of the local discontinuous Galerkin method for elliptic problems on cartesian grids*, SIAM J. Numer. Anal., 39 (2001), pp. 264–285.
- [7] H. GUO, L. TIAN, Z. XU, Y. YANG AND N. QI, *High-order local discontinuous Galerkin method for simulating wormhole propagation*, J. Comput. Appl. Math., 350 (2019), pp. 247–261.
- [8] H. GUO, R. JIA, L. TIAN AND Y. YANG, *Stability and error estimates of local discontinuous Galerkin method with implicit-explicit time marching for simulating wormhole propagation*, ESAIM Math. Model. Numer. Anal., 55 (2021), pp. 1103–1131.
- [9] S. HUBBARD, P. BABAK, S. SIGURDSSON AND K. MAGNUSSON, *A model of the formation of fish schools and migrations of fish*, Ecological Model., 174 (2004), pp. 359–374.
- [10] M. S. JIANG, J. S. ZHANG, J. ZHU, X. YU AND L. BEVILACQUA, *Numerical simulation for clustering and pattern formation in active colloids with mass-preserving characteristic finite element method*, Comput. Methods Appl. Mech. Eng., 381 (2021), p. 113806.
- [11] B. LIEBCHEN, D. MARENDUZZO, I. PAGONABARRAGA AND M. E. CATES, *Clustering and pattern formation in Chemorepulsive active colloids*, Phys. Rev. Lett., 115 (2015), p. 258301.
- [12] X. LI, C.-W. SHU AND Y. YANG, *Local discontinuous Galerkin methods for Keller-Segel chemotaxis model*, J. Sci. Comput., 73 (2017), pp. 943–967.
- [13] M. MUKHERJEE AND P. GHOSH, *Growth-mediated autochemotactic pattern formation in self-propelling bacteria*, Phys. Rev. E, 97 (2018), p. 012413.
- [14] E. RAUCH, M. MILLONAS AND D. CHIALVO, *Pattern formation and functionality in swarm models*, Phys. Lett. A, 207 (1995), pp. 185–193.
- [15] J. TONER AND Y. TU, *Long-range order in a two-dimensional dynamical XY model: how birds fly together*, Phys. Rev. Lett., 75 (1995), p. 4326.
- [16] D. E. WOODWARD, R. TYSON, M. R. MYERSCOUGH, J. D. MURRAY, E. O. BUDRENE AND H. C. BERG, *Spatio-temporal patterns generated by Salmonella typhimurium*, Biophys. J., 68 (1995), pp. 2181–2189.
- [17] H. WANG, Y. LIU, Q. ZHANG AND C.-W. SHU, *Local discontinuous Galerkin methods with implicit-explicit time-marching for time-dependent incompressible fluid flow*, Math. Comput., 88 (2019), pp. 91–121.
- [18] H. WANG, C.-W. SHU AND Q. ZHANG, *Stability and error estimates of local discontinuous Galerkin methods with implicit-explicit time-marching for advection-diffusion problems*, SIAM J. Numer. Anal., 53 (2015), pp. 206–227.
- [19] H. WANG, C.-W. SHU AND Q. ZHANG, *Stability analysis and error estimates of local discontinuous Galerkin methods with implicit-explicit time-marching for nonlinear convection-diffusion problems*, Appl. Math. Comput., 272 (2016), pp. 237–258.
- [20] H. WANG, S. WANG, Q. ZHANG AND C.-W. SHU, *Local discontinuous Galerkin methods with implicit-explicit time marching for multi-dimensional convection-diffusion problems*, ESAIM: M2AN, 50 (2016), pp. 1083–1105.
- [21] H. WANG, J. ZHENG, F. YU, H. GUO AND Q. ZHANG, *Local discontinuous Galerkin method with implicit-explicit time marching for incompressible miscible displacement problem in porous media*, J. Sci. Comput., 78 (2019), pp. 1–28.
- [22] Y. XU AND C.-W. SHU, *Local discontinuous Galerkin methods for high-order time-dependent partial differential equations*, Commun. Comput. Phys., 7(2010), pp. 1–46.